Dual loss of succinate dehydrogenase (SDH) and complex I activity is necessary to recapitulate the metabolic phenotype of SDH mutant tumors

Doriane Lorendeau[1,2], Gianmarco Rinaldi[1,2], Ruben Boon[3,4], Pieter Spincemaille[5], Kristine Metzger[1,2], Christian Jäger[6], Stefan Christen[1,2], Xiangyi Dong[6], Sabine Kuenen[7,8], Karin Voordeckers[9,10], Patrik Verstreken[7,8], David Cassiman[11], Pieter Vermeersch[5,12], Catherine Verfaillie[3,4], Karsten Hiller[6] & Sarah-Maria Fendt[1,2#]

[1]Laboratory of Cellular Metabolism and Metabolic Regulation, VIB Center for Cancer Biology, VIB Leuven, 3000 Leuven, Belgium

[2]Department of Oncology and Leuven Cancer Institute (LKI), KU Leuven, 3000 Leuven, Belgium

[3]Stem Cell Institute, KU Leuven, 3000 Leuven, Belgium

[4]Stem Cell Biology and Embryology Unit, Department of Development and Regeneration, KU Leuven, 3000 Leuven, Belgium

[5]Department of Laboratory Medicine, University Hospitals Leuven, 3000 Leuven, Belgium

[6]Luxembourg Centre for Systems Biomedicine, University of Luxembourg, 6, Avenue du Swing, L-4367 Belvaux, Luxembourg

[7]VIB Center for the Brain and Disease Research, VIB Leuven, 3000 Leuven, Belgium

[8]Department of Human Genetics and Leuven Research Institute for Neurodegenerative Diseases, KU Leuven, 3000 Leuven, Belgium

[9]Laboratory for Systems Biology, VIB Center for Microbiology, VIB Leuven, 3000 Leuven, Belgium

[10]CMPG Laboratory for Genetics and Genomics, KU Leuven, 3000 Leuven, Belgium.

[11]Department of Hepatology and Metabolic Center, University Hospitals Leuven, 3000 Leuven, Belgium

[12]Cardiology Department of Cardiovascular Sciences, KU Leuven, 3000 Leuven, Belgium

[#]corresponding author:
Sarah-Maria Fendt
VIB Center for Cancer Biology
Herestraat 49
3000 Leuven, Belgium
Tel: +32.16.37.32.61
e-mail: sarah-maria.fendt@vib-kuleuven.be

Keywords: succinate dehydrogenase; complex I of the electron transport chain; mitochondrial respiration; reductive glutamine metabolism; pyruvate carboxylase; ^{13}C metabolic flux analysis; paraganglioma; gastrointestinal stromal tumors; Leigh syndrome; ataxia; leukodystrophy; SDH mutations.

Chemical compounds studied in this article: 3-nitropropionic acid (PubChem CID: 1678), Atpenin A5 (PubChem CID: 54676868), rotenone (PubChem CID: 6758), CB-839 (PubChem CID: 71577426).

Abbreviations: 3-NPA, 3-nitropropionic acid; Co, complex; FH, fumarate hydratase; PC, pyruvate carboxylase; TCA cycle, tricarboxylic acid cycle; SDH, succinate dehydrogenase.

Highlights:

- Dual loss of SDH and complex I is required for the metabolism of SDH mutant tumors
- Loss of complex I impairs respiration in SDH-mutant cells
- Loss of complex I induces reductive glutamine metabolism in SDH-mutant cells
- Loss of complex I distinguishes SDH-mutant tumors versus SDH-mutant neurodegeneration
- Cells can sustain respiration upon a TCA cycle truncation at the level of SDH

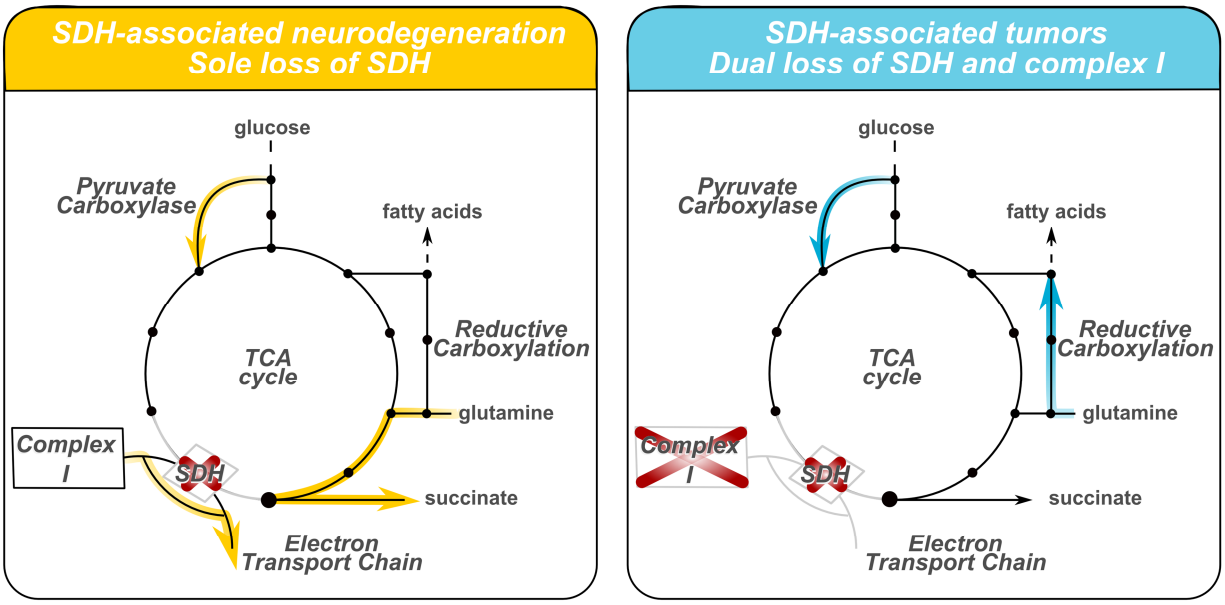

Mutations in succinate dehydrogenase (SDH) are associated with tumor development and neurodegenerative diseases. Only in tumors, loss of SDH activity is accompanied with the loss of complex I activity. Yet, it remains unknown whether the metabolic phenotype of SDH mutant tumors is driven by loss of complex I function, and whether this contributes to the peculiarity of tumor development versus neurodegeneration. We addressed this question by decoupling loss of SDH and complex I activity in cancer cells and neurons. We found that sole loss of SDH activity was not sufficient to recapitulate the metabolic phenotype of SDH mutant tumors, because it failed to decrease mitochondrial respiration and to activate reductive glutamine metabolism. These metabolic phenotypes were only induced upon the additional loss of complex I activity. Thus, we show that complex I function defines the metabolic differences between SDH mutation associated tumors and neurodegenerative diseases, which could open novel therapeutic options against both diseases.

1. Introduction

Oncogenic transformations of cells are directly connected to changes in metabolism (Elia et al. 2016). This is the case, because many tumor suppressors and oncogenes regulate metabolic enzymes (Elia et al. 2016). Thus, changes in metabolism are a consequence of the transformation process. Yet, metabolic changes can also be a cause of cellular transformation, because metabolites can regulate upstream signaling events by changing the activity state of oncogenes, tumor suppressors, and epigenetic regulators (Lorendeau et al. 2015). Examples of this latter class of transformation are mutations in TCA cycle enzymes (Nowicki and Gottlieb 2015). One of these enzymes is succinate dehydrogenase (SDH), which is mutated in a number of tumors such as paraganglioma and gastrointestinal stromal tumors (Evenepoel et al. 2015).

SDH consists of four subunits. SDHA contains the catalytic binding pocket for succinate and produces $FADH_2$ and fumarate within the TCA cycle. The electrons from $FADH_2$ are then funneled via SDHB to SDHC and SDHD, which constitute the complex II function within the electron transport chain. Mutations in each individual SDH subunit result in the accumulation of succinate, which leads to a deregulation of signaling and epigenetic events and thus an oncogenic transformation (Morin et al. 2014; Nowicki and Gottlieb 2015). Beyond the accumulation of succinate it has been shown that SDH knockout and mutant cells rely on increased pyruvate

carboxylase (PC)-dependent aspartate production and reductive glutamine metabolism (Lussey-Lepoutre et al. 2015; Cardaci et al. 2015; Saxena et al. 2016). Additionally, decreased mitochondrial respiration has been identified as a metabolic phenotype of SDH knockout and mutant cells (Rapizzi et al. 2015; Cardaci et al. 2015; Saxena et al. 2016). However, these latter alterations are also known consequences of complex I and III inhibition of the electron transport chain (Fendt et al. 2013a; Birsoy et al. 2015). Interestingly, SDH mutant tumors and SDH knockouts in cell lines show low or loss of complex I protein expression and activity (Favier et al. 2009; Cardaci et al. 2015). However it is unknown, whether the loss of SDH activity is sufficient to drive the metabolic phenotype of SDH mutant tumors or whether the accompanying loss of complex I activity also contributes to the specific metabolism of tumors associated with SDH mutations. Answering this question is of specific interest, because particular mutations in SDHA do not result in tumor development, but in neurodegenerative diseases such as Leigh syndrome, ataxia, and leukodystrophy (Hoekstra and Bayley 2013), and in these cases complex I activity is sustained (Burgeois et al. 1992; Bourgeron et al. 1995; Birch-Machin et al. 2000; Brockmann et al. 2002). Thus, complex I status in SDH mutant cells could support the disease prevalence of tumor development versus neurodegeneration.

To address the role of complex I activity in SDH mutation related diseases, we characterized the metabolic phenotype of SDHB knockout cells and a cell line harboring the tumor-associated SDHA R589W mutation, and compared them to cells treated with SDHA or B inhibitors (resulting in sustain complex I activity, but loss of SDH activity), complex I inhibitor, and cells harboring the neurodegeneration-associated SDHA R451C mutation. We found that sole inhibition of SDHA or B was sufficient to increase succinate accumulation and PC-dependent metabolism in various cell lines. However, inhibition of SDHA or B failed to effectively reduce mitochondrial respiration and to increase reductive glutamine metabolism. The latter metabolic alterations could only be induced by an additional complex I inhibition. Hence, with this study we revealed that loss of complex I activity is important for the metabolic phenotype of tumors that are associated with SDH mutations. Moreover, we provide evidence that in neurodegenerative diseases, that are defined by SDH mutation (and sustained complex I activity), mitochondrial respiration occurs and results in a high succinate secretion flux that has the potential to negatively affect disease prognosis.

2. Materials and methods

2.1 Cell culture conditions

Since so far no cancer patients-derived immortalized cell lines carrying SDH mutations (e.g. paraganglioma, gastro-intestinal stromal tumors derived cell lines) have been described, we used pharmacological inhibitors of SDH on several cancer cell lines or cell lines genetically engineered to carry SDH mutations or knockouts.

Hap1 cell line is a near-haploid human cell line derived from the male chronic myelogenous leukemia cell line (CML) KBM-7. Hap1 SDHA R589W cell line was generated with Haplogen company using a CRISPR/Cas9-based genome engineering strategy (Essletzbichler et al. 2014). Hap1 SDHA knockout (KO) + SDHA R451C overexpression and its control Hap1 SDHA KO + SDHA wildtype overexpression were generated as described in section *2.7*.

DU145 human prostate cancer cells were cultured in RPMI without pyruvate containing 10% dialyzed FBS and 1% penicilline/streptomycine. Huh7 human hepatocarcinoma cell line and HCT116 human colorectal carcinoma cell line were cultured in DMEM without pyruvate containing 10% dialyzed FBS and 1% penicilline/streptomycine. LUHMES mesencephalon neuronal cells were cultured and differentiated into dopaminergic neurons as described previously (Scholz et al. 2011). SDHB knockout (KO) mouse kidney cell lines, Hap1 cell lines and UOK262 human hereditary leiomyomatosis renal cell carcinoma (HLRCC) cell line were cultured in DMEM supplemented with 1 mM pyruvate, 10% dialyzed FBS and 1% penicilline/streptomycine. Additional nutrients (^{13}C labeled or unlabeled), or drugs were added 72h prior to cell harvest. The SDH inhibitor 3-nitropropionic acid (Sigma Aldrich #N5636) was applied at concentrations of 1 mM for LUHMES neurons and 5 mM for all other cell lines. The SDH inhibitor Atpenin A5 (Enzo life sciences #ALX-380-313) was applied at a concentration of 500 nM. 3-NPA can be considered as an SDHA inhibitor, as it binds in the FAD binding pocket of SDH subunit A (Sun et al. 2005). Atpenin A5 can be considered as an SDHB inhibitor, as it binds in the ubiquinone binding pocket comprised of residues from SDH subunit B, C and D (Horsefield et al. 2006). Complex I inhibitor rotenone (Sigma Aldrich #R8875) was applied at 20 ng ml^{-1}. Glutaminase inhibitor CB-839 (Calithera) was applied at a concentration of 100 nM. The dose-dependent effect of drugs, rotenone on complex I as monitored by inhibition of oxygen consumption and 3-NPA and Atpenin A5 on SDH as monitored by succinate accumulation, were

carried out to determine the dose of drugs that trigger significant inhibitory effects. Rotenone at 20 ng ml^{-1}, Atpenin A5 at 500 nM and 3-NPA at 1-5 mM was sufficient to reach significant inhibitory effect of the drugs on complex I and SDH in cancer cell lines, respectively (Supplemental Figure S1A-E).

2.2 ^{13}C tracer analysis

All labeling experiments were performed in dialyzed serum for 72h. $^{13}C_6$-glucose and $^{13}C_5$-glutamine tracers were purchased from Sigma-Aldrich. Metabolites for the subsequent mass spectrometry analysis were prepared by quenching the cells in liquid nitrogen followed by a cold two-phase methanol-water-chloroform extraction (Fendt et al. 2013a). Phase separation was achieved by centrifugation at 4 °C. The methanol-water phase containing polar metabolites was separated and dried using a vacuum concentrator. Dried metabolite samples were stored at -80 °C. Polar metabolites were derivatized for 90 min at 37 °C with 7.5 µl of 20 mg ml^{-1} methoxyamine in pyridine and subsequently for 60 min at 60 °C with 15 µl of N-(tert-butyldimethylsilyl)-N-methyltrifluoroacetamide, with 1% tert-butyldimethylchlorosilane (Fendt et al. 2013b) (Sigma-Aldrich). Fatty acids were esterified with sulphuric acid/methanol for 180 min at 60 °C and subsequently extracted with hexane. Isotopomer distributions and metabolite concentrations were measured with a 7890A GC system (Agilent Technologies) combined with a 5975C Inert MS system (Agilent Technologies). 1 µl of sample was injected into a DB35MS column in splitless mode using an inlet temperature of 270 °C. The carrier gas was helium with a flow rate of 1 ml min^{-1}. Upon injection, the GC oven was held at 100 °C for 3 min and then ramped to 300 °C with a gradient of 2.5 °C min^{-1} followed by a 5 min after run at 320 °C. For fatty acid samples, the oven was held at 80 °C for 1min and ramped with 5 °C min^{-1} to 300 °C. The MS system was operated under electron impact ionization at 70 eV and a mass range of 100–650 amu was scanned. Isotopomer distributions were extracted from the raw ion chromatograms using a custom Matlab M-file, which applies consistent integration bounds and baseline correction to each ion (Young et al. 2008). In addition, we corrected for naturally occurring isotopes using the method of Fernandez et al. (Fernandez et al. 1996). Negative values were considered as zero. We corrected the mass spectra for potential metabolite contamination in a blank extraction. All labeling fractions were transformed to a natural abundance corrected mass distribution vector (MDV) (Buescher et al. 2015).

PC-dependent metabolism was assessed as described before (Christen et al. 2016). Additional correction from pyruvate m+3 was performed when labeling experiment were performed in presence of pyruvate 1 mM for SDHB KO and SDHA R589W cell lines.

Metabolite concentrations were determined based on metabolite standard curve, the internal standards norvaline and glutarate, and cell numbers counted with a hemocytometer. Uptake and secretion rates of metabolite were determined based on the difference of metabolite concentrations in the media between 0h and 72h with or without drug treatment, normalized to the growth rates of cells.

Fractional contribution of 5-^{13}C-glutamine carbon source to fatty acid synthesis, D, and fractional new synthesis of fatty acids during time t, g(t), and total flux to fatty acid synthesis were estimated from the mass isotopomer distribution of palmitate based on isotopomer spectral analysis and palmitate concentrations as reported previously (Yoo et al. 2008; Fendt et al. 2013a).

Samples from LUHMES cells were analyzed using an Agilent 7890A GC coupled to an Agilent 5975C inert XL Mass Selective Detector (Agilent Technologies). The gas chromatograph was equipped with a 30 m (I.D. 250 µm, film 0.25 µm) DB-35MS capillary column including 5 m DuraGuard column in front of the analytical column (Agilent J&W GC Column). Helium was used as carrier gas with a constant flow rate of 1 ml min^{-1}. The GC oven temperature was held at 100 °C for 2 min and increased to 300 °C at 10 °C min^{-1} and held for 4 min. The total run time was 26 min. The transfer line temperature was set to 280 °C. The MSD was operating under electron ionization at 70 eV. The MS source was held at 230 °C and the quadrupole at 150 °C. Mass spectra were recorded in the range of m/z 70 to 800. All GC-MS chromatograms were processed using MetaboliteDetector, v3.020151231Ra. The software package supports automatic deconvolution of all mass spectra. Compounds were annotated by retention index and mass spectrum (Hiller et al. 2009).

2.3 ^{13}C metabolic flux model

Intracellular fluxes were estimated using the Matlab based software Metran (Antoniewicz et al. 2007; Young et al. 2008). Fluxes were modeled based on intracellular labeling of lactate, alanine, citrate, α-ketoglutarate, succinate, malate, aspartate, glutamate and glutamine from $^{13}C_6$-glucose tracer. We assumed that the system is in steady state. Unpublished data confirm that there is no

significant difference in the labeling of polar metabolites after 24h or 72h confirming the steady state assumption. Moreover, we assumed that all CO_2 in the system is unlabeled and that succinate has no orientation, because it is symmetrical. Additionally we assumed that any metabolite that is modeled in two different compartments is in equilibrium. The biomass fluxes were based on a previous publication and scaled by growth rate (Metallo et al. 2009). Entry of unlabeled glucose and acetyl-CoA precursors was assumed to be possible to account for fatty acid oxidation, glycogen stores, or entry of amino acids from the media. The pentose phosphate pathway flux was modeled as lower bound based on the flux to NTPs as described before (Lunt et al. 2015). Reductive glutamine metabolism was assumed to be cytosolic (Grassian et al. 2014). Glutamine to glutamate flux was calculated based on dynamic labeling data (Yuan et al. 2008; Buescher et al. 2015).

2.4 Oxygen consumption rates

Oxygen consumption was measured with an Oxytherm Clark electrode instrument (Hansatech). After a 72h treatment with 3-NPA 5 mM, Atpenin 500 nM, rotenone 20 ng ml^{-1}, or oligomycin A 1 µM over 24h, cells were trypsinized and resuspended in fresh media with at least $2x10^6$ cells for measurements. The oxygen consumption rate of cells in suspension was measured for 10 min at 37°C in the presence of the drugs. The slope of the linear range was used to calculate rates. Rates were calculated based on cell number counts using a hemocytometer. The ATP-coupled mitochondrial oxygen consumption rate is given by the difference between total oxygen consumption rates with or without SDH inhibitors (3-NPA, Atpenin A5) and oxygen consumption rates after oligomycin A treatment.

2.5 Enzymatic activity of electron transport chain complexes

The activity of citrate synthase and the individual complexes of the electron transport chain (complex I to complex IV) in cell lines was determined as described (Frazier and Thorburn 2012), with minor modifications on mitochondrial enriched fractions of the wild type versus mutant cell lines. Briefly, enriched mitochondrial fractions were prepared from snap frozen cell pellets by homogenization with a glass homogenizer and motor-driven teflon plunger in homogenization buffer containing HEPES, EGTA and sucrose. Subsequently, enriched mitochondrial fractions were prepared by differential centrifugation at 4°C (600*g* for 10 min to

obtain crude mitochondrial fraction in the supernatant, and subsequent 144000*g* for 10 min for the enriched fraction in the resulting pellet). Except for complex III activity, pellets were resuspended in hypotonic buffer containing potassium phosphate and $MgCl_2$. Citrate synthase and complex I-IV activities were determined by monitoring appearance or disappearance of specific substrates at specific wavelengths using spectrophotometry (e.g. oxidation of NADH for complex I activity at 340 nm in presence and absence of rotenone to evaluate complex I-specific activity, reduction of cytochrome c for complex III activity at 550 nm). A putative aspecific effect of pharmacological complex II inhibitors on other complexes activities was determined using the same technique. As such, the effect of 3-NPA (5 mM) and Atpenin (500 nM) on complex I, III and IV activities was determined by direct addition of the inhibitors to the cuvettes containing enriched mitochondrial fractions from DU145 cells. In order to draw general conclusions out of oxygen consumption rates (done on whole cells) and spectrophotometric enzymatic assays (done on mitochondrial extracts), we evaluated the mitochondrial abundance between cell lines by comparing citrate synthase activity on mitochondrial extracts with citrate synthase expression on whole cells (Supplemental Figure S2A-D). Since both measures provided similar results we normalized all measurements to protein and citrate synthase activity, to correct for mitochondrial abundance.

2.6 Western blotting

Cells were lysed in protein extraction buffer (25 mM Tris, 100 mM NaCl, 0.5% NP40, 0.5% deoxycholic acid, 5 mM EDTA, protease inhibitor cocktail (Sigma-Aldrich)). Aliquots of 50 µg of protein were separated on NuPAGE 4-12% denaturing Bis-Tris gels and transferred to nitrocellulose membranes (ThermoFisher Scientific). Antibodies used for western blot experiments were as follows, Oxphos complexes kit (Abcam ab110411), SDHA (ThermoFisher Scientific #459200), β-Actin (Sigma-Aldrich #A5441). The membranes were then incubated with horseradish peroxidase-linked mouse secondary antibodies (Cell Signaling Technology #7076) and bound antibodies were visualized using Pierce ECL reagent (ThermoFisher Scientific #32106).

2.7 Genetic manipulations

Hap1 SDHA R589W cell line was generated with Haplogen company using a CRISPR/Cas9-based genome engineering strategy (Essletzbichler et al. 2014). SDHA knockout (KO) targeting crispr plasmids were generated by cloning the crispr guides targeting exon 10 of SDHA in the lentiviral crispr and guide expressing plasmid lentiCRISPR v2(Plasmid #52961). 2 guides (GGAGTTTGCCCCGAGGCGGT and GTGCCCGACCAAAGACAACC) were designed using the MIT crispr design website (http://crispr.mit.edu/).

For SDHA R451C mutation and SDHA wt control, the SDHA ORF was bought as a gblock (Integrated DNA technologies) and cloned into the lentiviral pLVX-IRES-Hygromycin plasmid (Clontech, 632185) by gibson cloning using the NEbuilder kit (NEB, E5520S) (Table S1). Within the gblock the PAM sequences of the guides targeting SDHA were mutated with codon preservation. The SDHA R451C mutation was introduced by PCR (Table S1). Lentiviral particles for both the crispr KO vectors and the overexpression vectors were produced using a second generation lentiviral system using the psPAX2 packaging plasmid (Addgene Plasmid #12260) and the pMD2.G enveloppe plasmid (Addgene Plasmid #12259). Briefly, HEK293T cells were seeded at a density of $6x10^6$ cells in a 10 cm^2 dish with 10 ml of DMEM. After 24h incubation, cells were overlaid with the plasmids psPAX2 (packaging), pMD2.G (envelope) and PLVX-SDHA R451C or empty PLVX as control, together with optiMEM Lipofectamine 2000 (ratio 1/3 total DNA/lipofectamine, Thermo Fisher Scientific). After 48h post-infection the virus was harvested, filtered, and stored at -80°C. Recipient cell lines at a confluence of 70% were incubated overnight with medium containing 1/2 diluted virus and 8 μg ml^{-1} final concentration of hexadimethrine bromide (Sigma-Aldrich). After 24h of recovery, infected cells were selected with 800 μg ml^{-1} hygromycin B (Gibco). Guide efficiency for KO was screened by measuring succinate accumulation in the cells, guide 1 was used in all experiments. Overexpression of SDHA wt and SDHA R451C were verified based on gene expression (supplemental Figure S3).

2.8 qPCR

Total RNA was isolated from 2 to 10 mg of snap-frozen mouse liver tissue using lysing matrix D tubes (M Biomedicals) and TRIzol Reagent (Thermo Fisher Scientific) according to the manufacturer's protocol. Total RNA from cultured cell lines was isolated using the Purelink RNA Mini kit (Thermo Fisher Scientific). Single strand cDNA was synthetized from 1 μg of

total RNA using the qScript cDNA synthesis kit (Quantabio). Real-time quantitative PCR (RT-qPCR) was performed on a Viia7 instrument (Applied Biosystems) using a platinum SYBR green qPCR supermix UDG (Thermo Fisher Scientific). The denaturation step was performed at 95 °C for 5 min, and followed by PCR amplification of 40 cycles of denaturation at 95 °C for 15 s and annealing and extension at 60 °C for 45 s. The standard cDNA was obtained using the PCR mastermix 2X (Thermo Fisher Scientific) according to the manufacturer's protocol. The cDNA was loaded on a 1.5% agarose gel and run for 30 min at 135V. Afterwards, the cDNA was purified using the geneclean spin kit (Qbiogene) according to the manufacturer's protocol, and dilutions were made (1 pg up to 1-10 pg). Primers used for analysis are listed below:

Species	**Gene name**	**Primer direction**	**Sequence**
Human	SDHA	FW	5'-AGGAACCCGAGGTTTTCACT-3'
		RV	5'-CCTACCACCACTGCATCAAA-3'
Human	Citrate Synthase	FW	5'-TGCTTCCTCCACGAATTTGAAA-3'
		RV	5'-CCACCATACATCATGTCCACAG-3'
Mouse	Citrate Synthase	FW	5'-GGACAATTTTCCAACCAATCTGC-3'
		RV	5'-TCGGTTCATTCCCTCTGCATA-3'
Human	RPL19	FW	5'-AGTATGCTCAGGCTTCAGAAGA-3'
		RV	5'-ATTGGTCTCATTGGGGTCTAAC-3'
Mouse	RPL19	FW	5'-CAGGCATATGGGCATAGGGAA-3'
		RV	5'-TGCCTTCAGCTTGTGGATGT-3'

2.9 Statistical analysis

Statistical analysis was performed for each experiment on $n \geq 3$ biological replicates using a two-tailed paired t test with unequal variance for most of the experiments, except for enzymatic activities of electron transport chain complexes, where one-way ANOVA, Dunnett's multiple comparison test (H) and unpaired Student's t-test were used. $*p<0.05$, $**p<0.01$, $***p<0.001$ were used as symbols to represent significance levels. Either SEs or SDs were calculated as indicated in each figure legend.

3. Results

3.1 Paraganglioma-associated SDHA R589W mutation and SDHB knockout cells show a similar metabolic phenotype.

Sympathetic paragangliomas and pheochromocytomas are rare neuroendocrine tumors that are mostly benign. About 10-20% of these tumors become malignant, and approximately half among those malignant tumors have been found to carry hereditary germline mutations in *SDHB* (Jimenez et al. 2013). *SDHA* mutations have been mainly described in sporadic forms of these tumors (Burnichon et al. 2016). SDHB knockout and mutant cell lines have been investigated extensively. Yet, it remains unknown whether the same metabolic phenotypes that are found in SDHB knockout or mutant cell lines also occur when paraganglioma-associated mutations are located in SDHA. To test this, we generated with Haplogen an isogenic human Hap1 cancer cell line with SDHA R589W mutation, which was the first discovered SDHA mutation to be associated with the onset of paraganglioma tumors in patients and leads to a SDHA and B protein loss in tumor tissue (Burnichon et al. 2010). We compared the metabolic alterations in this cell line to the previously described SDHB knockout cell line (Cardaci et al. 2015). To conclude on the metabolic phenotype of these cell lines, we measured the intracellular concentration alterations of 20 metabolites of central carbon metabolism using mass spectrometry (Figure 1A). Both SDHB knockout cells and SDHA R589W cells displayed very similar metabolite level alterations, which included succinate accumulation, and fumarate as well as malate depletion, which is consistent with an impairment of SDH catalytic activity. Moreover, citrate and aspartate levels were also decreased, which indicates a switch to reductive glutamine metabolism and an increased requirement for PC-dependent aspartate production (Fendt et al. 2013a; Lussey-Lepoutre et al. 2015; Cardaci et al. 2015). To support our results from the metabolite concentration analysis, we next measured reductive glutamine and PC-dependent metabolism using 5-^{13}C-glutamine and $^{13}C_6$-glucose tracer analysis, respectively (Figure 1B-E). In line with our metabolomics results, we found that both SDHB knockout and SDHA R589W mutant cells showed increased reductive glutamine metabolism and PC-dependent metabolism.

Next, we quantified mitochondrial respiration in SDHB knockout and SDHA R589W cells based on ATP-coupled oxygen consumption rates measured with a Clark electrode, and the activity of the respiratory chain complexes based on spectrophotometric enzymatic assays (Figure 1F-I). As

expected from literature (Cardaci et al. 2015), SDHB knockout resulted in decreased ATP-coupled oxygen consumption rates and a loss of complex I, and II enzymatic activities. As expected from patient tissue (Burnichon et al. 2010), the insertion of the SDHA R589W mutation in Hap1 cells led to the loss of complex II activity. In addition, we found that SDHA R589W mutation in Hap1 cells showed a decreased cellular respiration and loss of complex I activity. Consequently we searched for the cause of the observed decreased complex I activity. Since SDHB knockout cells and paraganglioma patient samples were shown to have decreased expression of several electron transport chain complexes (Favier et al. 2009; Cardaci et al. 2015), we measured their protein expression in the Hap1 cells harboring the SDHA R589W mutation. We found that SDHA R589W cells showed an almost completely loss of complex I, SDHA, and SDHB protein expression (Figure 1J), which is consistent with decreased complexes activities. Taken together, we show that SDHB knockout and SDHA R589W mutant cells display a similar metabolic phenotype, which includes the loss of complex I activity. Thus, these data highlight the importance to assess which metabolic phenotype of SDH mutant tumors is driven by loss of SDH activity versus the accompanying loss of complex I activity.

3.2 Inhibition of SDHA or B activity does not result in decreased cellular respiration or increased reductive glutamine metabolism.

To test which metabolic phenotypes of tumors associated with SDH mutations are driven by loss of SDH versus complex I activity, we decoupled them using the SDHA inhibitor 3-nitropropionic acid (3-NPA) and the SDHB inhibitor Atpenin A5, which both do not inhibit complex I. First, we verified that both inhibitors only targeted SDH function represented by complex II activity, but not complex I activity based on spectrophotometric enzymatic assays in DU145 human prostate cancer cells (Figure 2A). As expected, complex II activity, (representing SDH function) decreased upon treatment with 3-NPA or Atpenin A5. In line with the known specificity of the pharmacologic inhibitors (Miyadera et al. 2003; Sun et al. 2005), we found that complex I, III, and, IV activities were not significantly altered upon treatment with either inhibitor (Figure 2A).

We next asked whether sole SDHA or B inhibition (without loss of complex I activity) is sufficient to induce the metabolic phenotype described for tumors associated with SDH mutations (succinate accumulation, increased reductive glutamine and pyruvate carboxylase

metabolism, as well as decreased cellular respiration). We determined the metabolic phenotype of cells upon treatment with 3-NPA and Atpenin A5 as described above. We found that sole SDHA or B inhibition was sufficient to induce succinate accumulation (>180 fold change to control for 3-NPA and >270 for Atpenin A5) (Figure 2B) and PC-dependent metabolism (Figure 2C). Unexpectedly however, we discovered that reductive glutamine metabolism and most surprisingly cellular respiration were hardly altered upon SDHA or B inhibition (Figure 2D and E). After verifying this unexpected metabolic phenotype in additional cell lines (Huh7 liver cancer cell line and HCT116 colon carcinoma cell line) (Supplemental Figure S4A-D), we investigated whether the observed cellular respiration was coupled to mitochondrial ATP production. We found that ATP-coupled respiration was only marginally decreased or unaltered (Figure 2F). Thus, we concluded that loss of SDH activity was sufficient to induce succinate accumulation and to increase PC-dependent metabolism, but failed to induce reductive glutamine metabolism and to inhibit mitochondrial respiration.

3.3 Dual loss of complex I and SDH activities recapitulate the metabolic phenotype of SDH mutant tumors.

Next, we asked whether loss of complex I activity is necessary to induce reductive glutamine metabolism and loss of cellular respiration in cells with inhibited SDH activity. To achieve complex I loss of activity we treated cells with the complex I inhibitor rotenone on top of 3-NPA or Atpenin A5 treatment and measured reductive glutamine metabolism and cellular respiration. We found that the additional loss of complex I in cancer cells with inhibition of SDHA or B resulted in decreased cellular respiration and increased reductive glutamine metabolism (Figure 3 A and B). In line with the observed increase in reductive glutamine metabolism, we found that rotenone treatment reduced the succinate secretion rate in 3-NPA or Atpenin A5 treated cells (Figure 3C). The comparison of the results from SDH and complex I inhibitor treated cells to only complex I inhibitor treated cells showed that the vast majority of the effects on reductive glutamine metabolism and cellular respiration were induced by complex I inhibition and not by a synergistic effect of SDH and complex I inhibition (Figure 3A and B). Thus, we concluded that dual loss of complex I and SDH activities is required to recapitulate the metabolic phenotype described for tumors associated with SDH mutations.

3.4 Succinate secretion flux is required for sustained cellular respiration upon SDHA inhibition.

Dual loss of SDH and complex I activity is only observed in tumors associated with SDH mutations (Favier et al. 2009; Cardaci et al. 2015), but not in neurodegenerative diseases associated with SDH mutations (Burgeois et al. 1992; Bourgeron et al. 1995; Birch-Machin et al. 2000; Brockmann et al. 2002). Thus, we next asked how respiration is sustained upon sole inhibition of SDH activity. To identify how cellular respiration is sustained upon loss of SDH activity we performed a ^{13}C metabolic flux analysis in cells treated with and without 3-NPA (Figure 4A, Table S2). The estimated flux data confirmed our above-obtained results, which were based on ^{13}C tracer analysis. In addition, we discovered that SDHA inhibition with 3-NPA significantly increased aspartate uptake, which is a metabolic alternative to PC-dependent *de novo* aspartate production. Moreover, we found that succinate accumulation upon SDHA inhibition was fueled mainly by glutamine metabolism, since glucose flux into the TCA cycle via pyruvate dehydrogenase was reduced by 2.8 fold, while glutamine anaplerosis was increased by 4 fold. This significant glutamine flux into the TCA cycle upon SDHA inhibition was sustained by a consecutive succinate secretion flux, which indicates that the combination of glutamine anaplerosis and succinate secretion fluxes produces the redox equivalents needed to maintain cellular respiration. To test this hypothesis we treated cells with 3-NPA and the glutaminase inhibitor CB-839, which inhibits glutamine flux into the TCA cycle. Subsequently, we measured the succinate secretion flux and cellular respiration (Figure 4B, C). Supporting our hypothesis that glutamine flux into the TCA cycle combined with succinate secretion flux sustains mitochondrial respiration upon inhibition of SDH activity, we found that succinate secretion flux and the oxygen consumption rate were decreased upon treatment with the glutaminase inhibitor.

Next, we tested whether it is possible to increase cellular respiration by inducing a succinate secretion flux. To do so we exploited another cancer associated TCA cycle enzyme alteration, namely the loss of fumarate hydratase (FH) in UOK262 cell lines. This alteration is found in specific forms of kidney cancer (human hereditary leiomyomatosis renal cell carcinoma) and leads to decreased cellular respiration (Yang et al. 2013; Nowicki and Gottlieb 2015). Thus, we hypothesized that treatment of fumarate hydratase null cells with 3-NPA initiates a succinate secretion flux and consequently cellular respiration. In agreement with this hypothesis, we found that 3-NPA treatment of fumarate hydratase null cells resulted in an increased succinate secretion flux (Figure 4D) and a two-fold increase in cellular respiration (Figure 4E). Notably, 3-NPA

treatment induced cellular respiration even reached 70% of the maximal possible cellular respiration, which was measured in UOK262 cells re-expressing fumarate hydratase (Figure 4E). Based on this data we concluded that cellular respiration is possible in cells with loss of SDH activity via a sustained succinate secretion flux. Moreover, this finding implies that decreased versus sustained cellular respiration is a major metabolic difference between tumors and neurodegenerative diseases associated with SDH mutations.

3.5 SDHA inhibition in neurons and in cells with neurodegeneration-associated SDHA R451C mutation results in sustained cellular respiration

To further support our hypothesis that deficiency in SDH activity associated with neurodegenerative diseases result in sustained cellular respiration, we tested whether SDHA inhibition in post-mitotic neuronal cells (differentiated LUHMES cell line) and overexpression of the neurodegeneration-associated SDHA R451C mutation in Hap1 cells results in succinate accumulation and sustained cellular respiration. In line with our hypothesis we found that SDHA inhibition by 3-NPA in differentiated LUHMES cells and overexpression of SDHA R451C in Hap1 cells induced succinate accumulation (Figure 5A and B), and resulted in sustained cellular respiration (Figure 5C and D).

Next, we tested whether reductive glutamine metabolism was induced in differentiated LUHMES cells upon SDHA inhibition and in SDHA R451C overexpressing Hap1 cells. Since *de novo* fatty acids synthesis is limited in post-mitotic neurons, we investigated the $^{13}C_5$-glutamine contribution to citrate and malate. We specifically focused on the ratios of M+5/M+4 citrate and M+3/M+4 malate from $^{13}C_5$-glutamine, which are indicative of a change in reductive glutamine metabolism (Fendt et al. 2013a). We found that upon 3-NPA treatment both ratios were decreased (Figure 5E and F), indicating that upon SDHA inhibition differentiated LUHMES neurons did not induce reductive glutamine metabolism. To assess reductive glutamine metabolism in the SDHA R451C overexpressing Hap1 cells, we determined the contribution of 5-^{13}C-glutamine to palmitate production as described above. In line with the results from LUHMES cells with inhibited SDHA activity, we found that SDHA R451C overexpression in Hap1 cells only marginally induces reductive glutamine metabolism (Figure 5G). Thus, differently from tumor-associated SDH mutations, SDH inhibition in neurons and

SDHA mutations associated with neurodegenerative diseases resulted in sustained respiration and no significant induction of reductive glutamine metabolism.

In conclusion, our findings suggest that the complex I activity together with the resulting metabolic alterations is a major difference of cells harboring SDH mutations associated with tumors versus SDH mutations associated with neurodegenerative diseases.

4. Discussion

Mutations in SDH are associated with rare tumors and neurodegenerative diseases. Here, we investigated whether loss of SDH activity is sufficient to induce the metabolic phenotype described for tumors with SDH mutation. We found that only a part of the tumor-associated metabolic phenotype is induced by loss of SDH activity. Full recapitulation of the described phenotype is only achieved by a dual loss of SDH and complex I activity. Our finding can consequently explain how SDH mutations can be associated with tumors, but also with neurodegenerative diseases, since the latter are defined by a sole decrease of SDH activity, but sustained complex I activity.

SDH mutations found in tumors are coupled to an additional loss in complex I activity of the electron transport chain (Favier et al. 2009; Cardaci et al. 2015). However, loss of complex I activity is not observed for neurodegenerative diseases that are associated with SDH mutations (Burgeois et al. 1992; Bourgeron et al. 1995; Birch-Machin et al. 2000; Brockmann et al. 2002). A previous study found evidence that differential accumulation of ROS contributes to the cancer versus neurodegeneration association of SDH mutations (Guzy et al. 2008). Beyond this study we discovered that the metabolic phenotype of cells with SDH mutations associated with tumors or neurodegenerative diseases differs because of their differential complex I activity status. One can speculate that the additional loss of complex I activity, and thus the decrease in respiration (and increase in reductive glutamine metabolism) in tumors associated with SDH mutations is needed to allow redirecting carbon flow towards biomass precursor production. This speculation is in line with our finding that sole inhibition of SDH activity leads to almost complete proliferation inhibition in various cancer cell lines (data not shown).

Many neurodegenerative diseases are accompanied by an intra- and extracellular accumulation of succinate, which can repress the response of neurons to neurotransmitters such as acetylcholine (Andreev et al. 1986). Our finding that an inhibition of complex I in cells with loss of SDH activity reduces succinate intra- and extracellular accumulation, provides a mechanistic explanation for the observation that metformin, an antidiabetic drug which inhibits complex I (Fendt et al. 2013b), attenuates the progression of neurodegenerative diseases that are accompanied by succinate accumulation such as Huntington's disease (Ma et al. 2007; Verwaest et al. 2011). Thus, it can be speculated that metformin treatment might also be beneficial to counteract disease progression in neurodegenerative diseases associated with SDH mutations. Additionally, it has been found that mTORC1 inhibition alleviates Leigh syndrome, which is frequently associated with SDH mutations (Johnson et al. 2013). mTORC1 is a known activator of glutamine flux into the TCA cycle (Csibi et al. 2013; Csibi et al. 2014). Thus, our finding that inhibition of glutaminase reduces succinate secretion flux in cells with impaired SDH function indicates that part of the beneficial effect of mTORC1 inhibition on Leigh syndrome symptoms can be explained by a reduction in glutamine-fueled succinate production and succinate secretion flux. Consequently, glutaminase inhibitors, which have been developed in the cancer research field (Elia et al. 2016), might have the potential to be a more targeted and effective therapy to inhibit the disease progression in Leigh syndrome patients with SDH mutations.

In conclusion, our study shows that a dual loss of SDH and complex I function is necessary to explain the so far described metabolic phenotype of tumors associated with SDH mutations. Moreover, our study provides evidence that the obstacle how SDH mutations can be associated with both, tumors and neurodegeneration, can be explained by the additional loss of complex I activity in tumors (but not in neurodegerative diseases), which rewires metabolism presumably to allow proliferation. Consequently, our data suggest that reactivation of respiration in tumors associated with SDH mutations could inhibit their proliferation, while induction of complex I inhibition could be beneficial to counteract disease progression in patients with neurodegenerative diseases that are associated with SDH mutations.

Acknowledgements

We thank Prof. Marston Linehan (NCI) and Prof. Eyal Gottlieb (Technion) for sharing with us the FH null cells, and the SDHB knockout cells, respectivley. We thank Prof. Julian Aragones Lopez (Madrid Autonomous University) and Prof. Ralph DeBerardinis (UT Southwestern) for kindly providing reagents. DL is supported by a VIB-Marie Curie fellowship. DC and PiV have senior clinical investigator fellowships of the FWO Flanders. KV is supported by a FWO postdoctoral fellowship. SMF acknowledges funding support from Marie Curie – CIG, FWO – Odysseus II, Concern Foundation, FWO – Research Grants, KU-Leuven Methusalem co-funding, Eugène Yourassowsky Schenking, and Bayer Health Care.

Author contribution

DL, GR, RB, PS, XD, KM, SC, and CJ performed experiments. DL, GR, SC, PS, CJ and SMF analyzed data. RB, SK, KV, CV and PaV supported genetic engineering. DC and PiV supervised enzymatic assays. KH supervised experiments with neurons. DL and SMF drafted the manuscript. SMF conceived, designed, and supervised the study. All authors have read and approved the manuscript.

Competing interest

The authors declare that they have no conflict of interest.

References

Andreev, A. A., C. A. Vulfius, A. Budantsev, M. N. Kondrashova, and E. V. Grishina. (1986) Depression of neuron responses to acetylcholine by combined application of norepinephrine and substrates of the tricarboxylic acid cycle. Cell Mol Neurobiol **6**(4): 407-20.

Antoniewicz, M. R., J. K. Kelleher, and G. Stephanopoulos. (2007) Elementary metabolite units (EMU): a novel framework for modeling isotopic distributions. Metab Eng **9**(1): 68-86.

Birch-Machin, M. A., R. W. Taylor, B. Cochran, B. A. Ackrell, and D. M. Turnbull. (2000) Late-onset optic atrophy, ataxia, and myopathy associated with a mutation of a complex II gene. Ann Neurol **48**(3): 330-5.

Birsoy, K., T. Wang, W. W. Chen, E. Freinkman, M. Abu-Remaileh, and D. M. Sabatini. (2015) An Essential Role of the Mitochondrial Electron Transport Chain in Cell Proliferation Is to Enable Aspartate Synthesis. Cell **162**(3): 540-51.

Bourgeron, T., P. Rustin, D. Chretien, M. Birch-Machin, M. Bourgeois, E. Viegas-Pequignot, A. Munnich, and A. Rotig. (1995) Mutation of a nuclear succinate dehydrogenase gene results in mitochondrial respiratory chain deficiency. Nat Genet **11**(2): 144-9.

Brockmann, K., A. Bjornstad, P. Dechent, C. G. Korenke, J. Smeitink, J. M. Trijbels, S. Athanassopoulos, R. Villagran, O. H. Skjeldal, E. Wilichowski, J. Frahm, and F. Hanefeld. (2002) Succinate in dystrophic white matter: a proton magnetic resonance spectroscopy finding characteristic for complex II deficiency. Ann Neurol **52**(1): 38-46.

Buescher, J. M., M. R. Antoniewicz, L. G. Boros, S. C. Burgess, H. Brunengraber, C. B. Clish, R. J. DeBerardinis, O. Feron, C. Frezza, B. Ghesquiere, E. Gottlieb, K. Hiller, R. G. Jones, J. J. Kamphorst, R. G. Kibbey, A. C. Kimmelman, J. W. Locasale, S. Y. Lunt, O. D. Maddocks, C. Malloy, C. M. Metallo, E. J. Meuillet, J. Munger, K. Noh, J. D. Rabinowitz, M. Ralser, U. Sauer, G. Stephanopoulos, J. St-Pierre, D. A. Tennant, C. Wittmann, M. G. Vander Heiden, A. Vazquez, K. Vousden, J. D. Young, N. Zamboni, and S. M. Fendt. (2015) A roadmap for interpreting (13)C metabolite labeling patterns from cells. Curr Opin Biotechnol **34**: 189-201.

Burgeois, M., F. Goutieres, D. Chretien, P. Rustin, A. Munnich, and J. Aicardi. (1992) Deficiency in complex II of the respiratory chain, presenting as a leukodystrophy in two sisters with Leigh syndrome. Brain Dev **14**(6): 404-8.

Burnichon, N., J. J. Briere, R. Libe, L. Vescovo, J. Riviere, F. Tissier, E. Jouanno, X. Jeunemaitre, P. Benit, A. Tzagoloff, P. Rustin, J. Bertherat, J. Favier, and A. P. Gimenez-Roqueplo. (2010) SDHA is a tumor suppressor gene causing paraganglioma. Hum Mol Genet **19**(15): 3011-20.

Burnichon, N., A. Buffet, and A. P. Gimenez-Roqueplo. (2016) Pheochromocytoma and paraganglioma: molecular testing and personalized medicine. Curr Opin Oncol **28**(1): 5-10.

Cardaci, S., L. Zheng, G. MacKay, N. J. van den Broek, E. D. MacKenzie, C. Nixon, D. Stevenson, S. Tumanov, V. Bulusu, J. J. Kamphorst, A. Vazquez, S. Fleming, F. Schiavi, G. Kalna, K. Blyth, D. Strathdee, and E. Gottlieb. (2015) Pyruvate carboxylation enables growth of SDH-deficient cells by supporting aspartate biosynthesis. Nat Cell Biol **17**(10): 1317-26.

Christen, S., D. Lorendeau, R. Schmieder, D. Broekaert, K. Metzger, K. Veys, I. Elia, J. M. Buescher, M. F. Orth, S. M. Davidson, T. G. Grunewald, K. De Bock, and S. M. Fendt. (2016) Breast Cancer-Derived Lung Metastases Show Increased Pyruvate Carboxylase-Dependent Anaplerosis. Cell Rep **17**(3): 837-48.

Csibi, A., S.-M. Fendt, C. Li, G. Poulogiannis, A. Y. Choo, D. J. Chapski, S. M. Jeong, J. M. Dempsey, A. Parkhitko, T. Morrison, E. P. Henske, M. C. Haigis, L. C. Cantley, G. Stephanopoulos, J. Yu, and J. Blenis. (2013) The mTORC1 pathway stimulates glutamine metabolism and cell proliferation by repressing SIRT4. Cell **153**(4): 840-54.

Csibi, A., G. Lee, S.-O. Yoon, H. Tong, D. Ilter, I. Elia, S.-M. Fendt, Thomas M. Roberts, and J. Blenis. (2014) The mTORC1/S6K1 Pathway Regulates Glutamine Metabolism through the eIF4B-Dependent Control of c-Myc Translation. Current Biology **24**(19): 2274-80.

Elia, I., R. Schmieder, S. Christen, and S. M. Fendt. (2016) Organ-Specific Cancer Metabolism and Its Potential for Therapy. Handb Exp Pharmacol **233**: 321-53.

Essletzbichler, P., T. Konopka, F. Santoro, D. Chen, B. V. Gapp, R. Kralovics, T. R. Brummelkamp, S. M. Nijman, and T. Burckstummer. (2014) Megabase-scale deletion using CRISPR/Cas9 to generate a fully haploid human cell line. Genome Res **24**(12): 2059-65.

Evenepoel, L., T. G. Papathomas, N. Krol, E. Korpershoek, R. R. de Krijger, A. Persu, and W. N. Dinjens. (2015) Toward an improved definition of the genetic and tumor spectrum associated with SDH germ-line mutations. Genet Med **17**(8): 610-20.

Favier, J., J. J. Briere, N. Burnichon, J. Riviere, L. Vescovo, P. Benit, I. Giscos-Douriez, A. De Reynies, J. Bertherat, C. Badoual, F. Tissier, L. Amar, R. Libe, P. F. Plouin, X. Jeunemaitre, P. Rustin, and A. P. Gimenez-Roqueplo. (2009) The Warburg effect is genetically determined in inherited pheochromocytomas. PLoS One **4**(9): e7094.

Fendt, S. M., E. L. Bell, M. A. Keibler, B. A. Olenchock, J. R. Mayers, T. M. Wasylenko, N. I. Vokes, L. Guarente, M. G. Vander Heiden, and G. Stephanopoulos. (2013a) Reductive glutamine metabolism is a function of the alpha-ketoglutarate to citrate ratio in cells. Nat Commun **4**: 2236.

Fendt, S. M., E. L. Bell, M. A. Keibler, S. M. Davidson, G. J. Wirth, B. Fiske, J. R. Mayers, M. Schwab, G. Bellinger, A. Csibi, A. Patnaik, M. J. Blouin, L. C. Cantley, L. Guarente, J. Blenis, M. N. Pollak, A. F. Olumi, M. G. Vander Heiden, and G. Stephanopoulos. (2013b) Metformin decreases glucose oxidation and increases the dependency of prostate cancer cells on reductive glutamine metabolism. Cancer Res **73**(14): 4429-38.

Fernandez, C. A., C. Des Rosiers, S. F. Previs, F. David, and H. Brunengraber. (1996) Correction of 13C mass isotopomer distributions for natural stable isotope abundance. J Mass Spectrom **31**(3): 255-62.

Frazier, A. E. and D. R. Thorburn. (2012) Biochemical analyses of the electron transport chain complexes by spectrophotometry. Methods Mol Biol **837**: 49-62.

Grassian, A. R., S. J. Parker, S. M. Davidson, A. S. Divakaruni, C. R. Green, X. Zhang, K. L. Slocum, M. Pu, F. Lin, C. Vickers, C. Joud-Caldwell, F. Chung, H. Yin, E. D. Handly, C. Straub, J. D. Growney, M. G. Vander Heiden, A. N. Murphy, R. Pagliarini, and C. M. Metallo. (2014) IDH1 Mutations Alter Citric Acid Cycle Metabolism and Increase Dependence on Oxidative Mitochondrial Metabolism. Cancer Res **74**(12): 3317-31.

Guzy, R. D., B. Sharma, E. Bell, N. S. Chandel, and P. T. Schumacker. (2008) Loss of the SdhB, but Not the SdhA, subunit of complex II triggers reactive oxygen species-dependent hypoxia-inducible factor activation and tumorigenesis. Mol Cell Biol **28**(2): 718-31.

Hiller, K., J. Hangebrauk, C. Jager, J. Spura, K. Schreiber, and D. Schomburg. (2009) MetaboliteDetector: comprehensive analysis tool for targeted and nontargeted GC/MS based metabolome analysis. Anal Chem **81**(9): 3429-39.

Hoekstra, A. S. and J. P. Bayley. (2013) The role of complex II in disease. Biochim Biophys Acta **1827**(5): 543-51.

Horsefield, R., V. Yankovskaya, G. Sexton, W. Whittingham, K. Shiomi, S. Omura, B. Byrne, G. Cecchini, and S. Iwata. (2006) Structural and computational analysis of the quinone-binding site of complex II (succinate-ubiquinone oxidoreductase): a mechanism of electron transfer and proton conduction during ubiquinone reduction. J Biol Chem **281**(11): 7309-16.

Jimenez, C., E. Rohren, M. A. Habra, T. Rich, P. Jimenez, M. Ayala-Ramirez, and E. Baudin. (2013) Current and future treatments for malignant pheochromocytoma and sympathetic paraganglioma. Curr Oncol Rep **15**(4): 356-71.

Johnson, S. C., M. E. Yanos, E.-B. Kayser, A. Quintana, M. Sangesland, A. Castanza, L. Uhde, J. Hui, V. Z. Wall, A. Gagnidze, K. Oh, B. M. Wasko, F. J. Ramos, R. D. Palmiter, P. S. Rabinovitch, P. G. Morgan, M. M. Sedensky, and M. Kaeberlein. (2013) mTOR Inhibition Alleviates Mitochondrial Disease in a Mouse Model of Leigh Syndrome. Science **342**(6165): 1524-28.

Lorendeau, D., S. Christen, G. Rinaldi, and S. M. Fendt. (2015) Metabolic control of signalling pathways and metabolic auto-regulation. Biol Cell **107**(8): 251-72.

Lunt, S., V. Muralidhar, Aaron M. Hosios, William J. Israelsen, Dan Y. Gui, L. Newhouse, M. Ogrodzinski, V. Hecht, K. Xu, Paula N. M. Acevedo, Daniel P. Hollern, G. Bellinger, Talya L. Dayton, S. Christen, I. Elia, Anh T. Dinh, G. Stephanopoulos, Scott R. Manalis, Michael B. Yaffe, Eran R. Andrechek, S.-M. Fendt, and Matthew G. Vander Heiden. (2015) Pyruvate Kinase Isoform Expression Alters Nucleotide Synthesis to Impact Cell Proliferation. Molecular Cell **57**(1): 95-107.

Lussey-Lepoutre, C., K. E. Hollinshead, C. Ludwig, M. Menara, A. Morin, L. J. Castro-Vega, S. J. Parker, M. Janin, C. Martinelli, C. Ottolenghi, C. Metallo, A. P. Gimenez-Roqueplo, J. Favier, and D. A. Tennant. (2015) Loss of succinate dehydrogenase activity results in dependency on pyruvate carboxylation for cellular anabolism. Nat Commun **6**: 8784.

Ma, T. C., J. L. Buescher, B. Oatis, J. A. Funk, A. J. Nash, R. L. Carrier, and K. R. Hoyt. (2007) Metformin therapy in a transgenic mouse model of Huntington's disease. Neuroscience Letters **411**(2): 98-103.

Metallo, C. M., J. L. Walther, and G. Stephanopoulos. (2009) Evaluation of 13C isotopic tracers for metabolic flux analysis in mammalian cells. J Biotechnol **144**(3): 167-74.

Miyadera, H., K. Shiomi, H. Ui, Y. Yamaguchi, R. Masuma, H. Tomoda, H. Miyoshi, A. Osanai, K. Kita, and S. Omura. (2003) Atpenins, potent and specific inhibitors of mitochondrial complex II (succinate-ubiquinone oxidoreductase). Proc Natl Acad Sci U S A **100**(2): 473-7.

Morin, A., E. Letouze, A. P. Gimenez-Roqueplo, and J. Favier. (2014) Oncometabolites-driven tumorigenesis: From genetics to targeted therapy. Int J Cancer **135**(10): 2237-48.

Nowicki, S. and E. Gottlieb. (2015) Oncometabolites: tailoring our genes. FEBS J **282**(15): 2796-805.

Rapizzi, E., R. Fucci, E. Giannoni, L. Canu, S. Richter, P. Cirri, and M. Mannelli. (2015) Role of microenvironment on neuroblastoma SK-N-AS SDHB-silenced cell metabolism and function. Endocr Relat Cancer **22**(3): 409-17.

Saxena, N., N. Maio, D. R. Crooks, C. J. Ricketts, Y. Yang, M. H. Wei, T. W. Fan, A. N. Lane, C. Sourbier, A. Singh, J. K. Killian, P. S. Meltzer, C. D. Vocke, T. A. Rouault, and W. M. Linehan. (2016) SDHB-Deficient Cancers: The Role of Mutations That Impair Iron Sulfur Cluster Delivery. J Natl Cancer Inst **108**(1).

Scholz, D., D. Poltl, A. Genewsky, M. Weng, T. Waldmann, S. Schildknecht, and M. Leist. (2011) Rapid, complete and large-scale generation of post-mitotic neurons from the human LUHMES cell line. J Neurochem **119**(5): 957-71.

Sun, F., X. Huo, Y. Zhai, A. Wang, J. Xu, D. Su, M. Bartlam, and Z. Rao. (2005) Crystal structure of mitochondrial respiratory membrane protein complex II. Cell **121**(7): 1043-57.

Verwaest, K. A., T. N. Vu, K. Laukens, L. E. Clemens, H. P. Nguyen, B. Van Gasse, J. C. Martins, A. Van Der Linden, and R. Dommisse. (2011) 1H NMR based metabolomics of CSF and blood serum: A metabolic profile for a transgenic rat model of Huntington disease. Biochimica et Biophysica Acta (BBA) - Molecular Basis of Disease **1812**(11): 1371-79.

Yang, Y., A. N. Lane, C. J. Ricketts, C. Sourbier, M. H. Wei, B. Shuch, L. Pike, M. Wu, T. A. Rouault, L. G. Boros, T. W. Fan, and W. M. Linehan. (2013) Metabolic reprogramming for producing energy and reducing power in fumarate hydratase null cells from hereditary leiomyomatosis renal cell carcinoma. PLoS One **8**(8): e72179.

Yoo, H., M. R. Antoniewicz, G. Stephanopoulos, and J. K. Kelleher. (2008) Quantifying Reductive Carboxylation Flux of Glutamine to Lipid in a Brown Adipocyte Cell Line. Journal of Biological Chemistry **283**(30): 20621-27.

Young, J. D., J. L. Walther, M. R. Antoniewicz, H. Yoo, and G. Stephanopoulos. (2008) An elementary metabolite unit (EMU) based method of isotopically nonstationary flux analysis. Biotechnol Bioeng **99**(3): 686-99.

Yuan, J., B. D. Bennett, and J. D. Rabinowitz. (2008) Kinetic flux profiling for quantitation of cellular metabolic fluxes. Nat Protoc **3**(8): 1328-40.

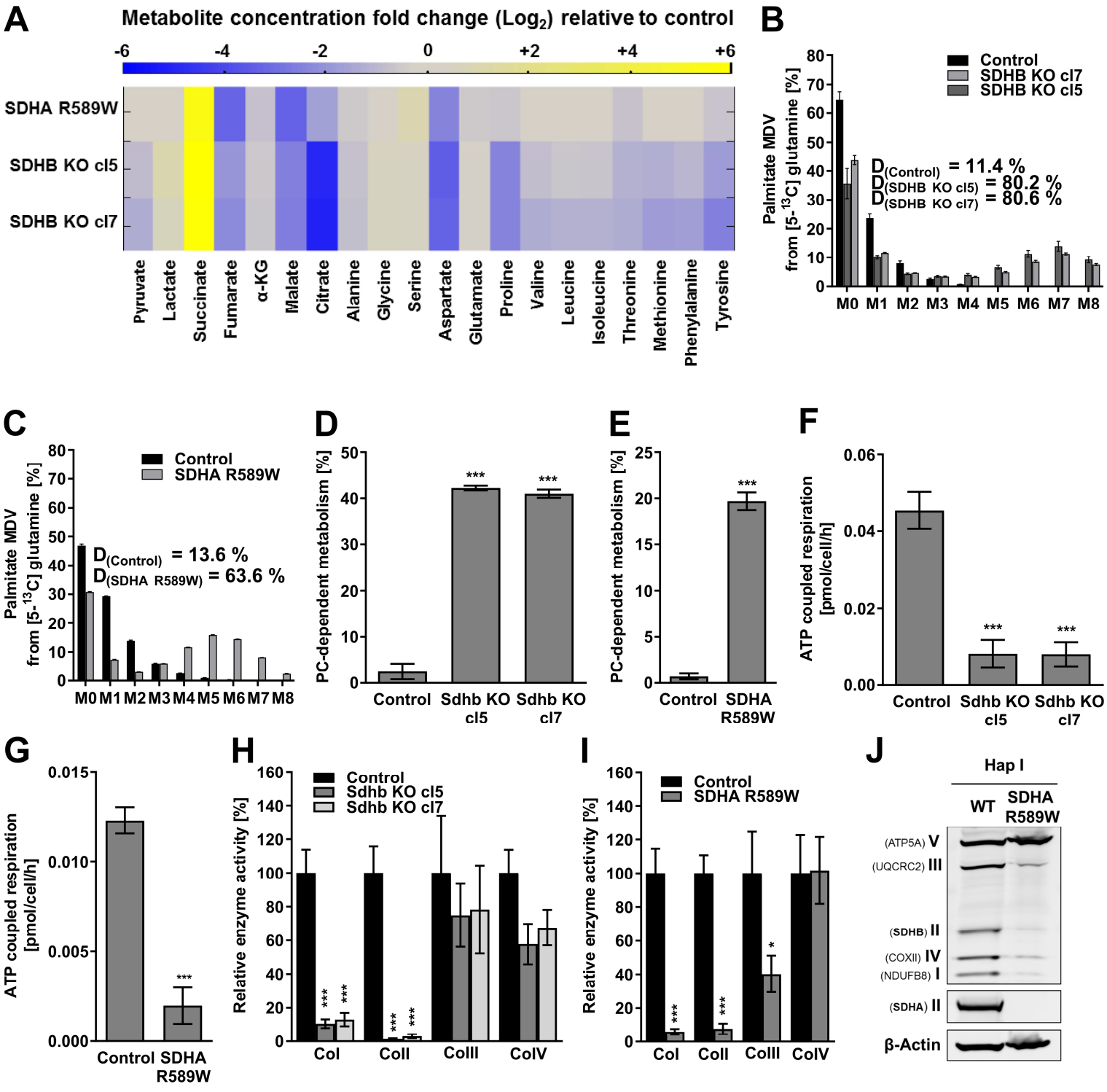

Figure 1 Paraganglioma-associated SDHA R589W mutation and SDHB knockout cells show a similar metabolic phenotype

(A) Fold change of intracellular metabolite concentrations of SDHB knockout (KO) in mouse kidney and SDHA R589W Hap1 cell lines compared to the corresponding wild type cell lines. cl refers to the different clones of the generated cell lines. **(B-C)** Reductive glutamine metabolism based on the contribution of 5-^{13}C-glutamine to palmitate. D values represent the fraction of newly synthesized palmitate that was produced from reductive glutamine metabolism in SDHB knockout (KO) mouse kidney and SDHA R589W Hap1 cell lines. Cells were incubated in medium containing 4 mM 5-^{13}C-glutamine tracer for 72h. All 95% confidence intervals were ≤ 3.8%. **(D-E)** PC-dependent metabolism in SDHB knockout (KO) mouse kidney and SDHA R589W Hap1 cell lines. PC-dependent metabolism was assessed based on the difference between malate and succinate M+3 divided by pyruvate M+3 from $^{13}C_6$-glucose to correct for label dilution due to growth in presence of 1 mM pyruvate. **(F-G)** ATP-coupled respiration in SDHB knockout (KO) mouse kidney and SDHA R589W Hap1 cell lines. ATP-coupled respiration was assessed by the difference between total oxygen consumption rate and oxygen consumption rate in the presence of the ATP synthase inhibitor oligomycin A 1 μM. **(H-I)** Relative enzyme activities of electron transport chain complexes I to IV to the control in SDHB knockout (KO) mouse kidney and SDHA R589W Hap1 cell lines. Assays were performed on mitochondrial membrane fractions prepared from the cells. Complexes activities were normalized to the control, protein quantity and citrate synthase (CS) activity. Complex I specific activity was determined by subtracting the total complex I activity from the rotenone-sensitive complex I activity. **(J)** Expression levels of proteins of mitochondrial complexes I (NDUFB8 subunit), II (SDHB and SDHA), III (Core 2 UQCRC2), IV (Cox II) and ATP synthase (ATP5A) in SDHA R589W Hap 1 cells compared to the wild type control cell line, as determined by western blot.

Error bars depict either SD (B-G) or SE (H-I). Statistical analysis was performed for each experiment on n≥3 biological replicates using a two-tailed paired t test with unequal variance (B-G), one-way ANOVA, Dunnett's multiple comparison test (H) and unpaired Student's t-test (I) were used. *$p<0.05$, ***$p<0.001$ represent p-values significance.

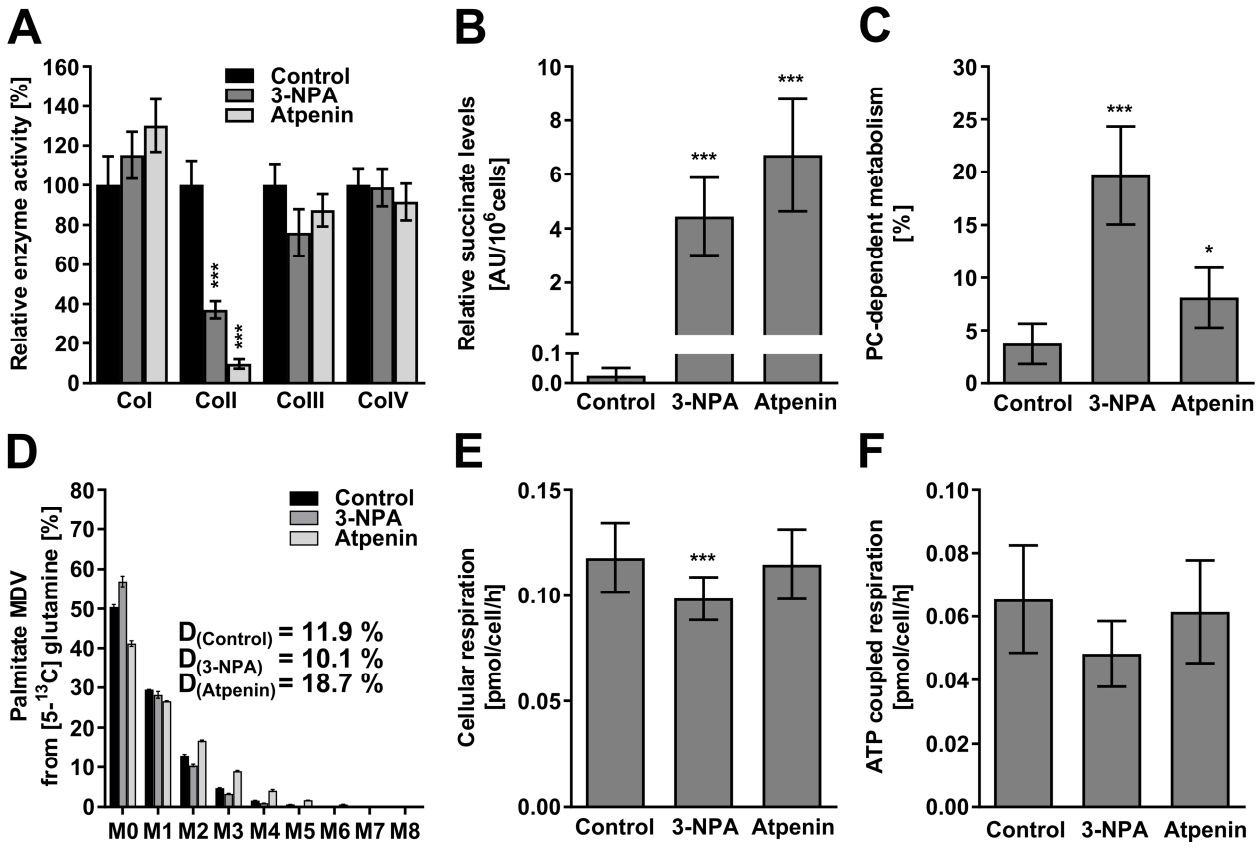

Figure 2 Inhibition of SDHA or B activity does not result in decreased cellular respiration or increased reductive glutamine metabolism

(A) Relative enzyme activities of electron transport chain complexes I to IV in DU145 prostate cancer cells. Assays were performed on cellular enriched mitochondrial fractions and in presence of SDH inhibitors 3-NPA 5 mM or Atpenin A5 500 nM. Complexes activities were normalized to the control, protein quantity, and citrate synthase (CS) activity. Complex I specific activity was determined by subtracting the total complex I activity from the rotenone-sensitive complex I activity. **(B)** Relative succinate levels in DU145 cells treated with SDH inhibitors 3-NPA or Atpenin A5. **(C)** PC-dependent metabolism in DU145 with 3-NPA or Atpenin A5. PC-dependent anaplerosis was assessed based on the difference between malate M+3 and succinate M+3 from $^{13}C_6$-glucose. **(D)** Reductive glutamine metabolism based on the contribution of 5-^{13}C-glutamine to palmitate. D values represent the fraction of newly synthesized palmitate that was produced from reductive glutamine metabolism in DU145 cells treated with 3-NPA or Atpenin A5 upon incubation in medium containing 2 mM 5-^{13}C-glutamine tracer for 72h. All 95% confidence intervals were ≤ 0.93%. **(E)** Cellular respiration measured in DU145 cells treated with 3-NPA or

Atpenin A5. (**F**) ATP-coupled respiration in DU145 treated with 3-NPA or Atpenin A5. ATP-coupled respiration was assessed by the difference between total oxygen consumption rates and oxygen consumption rates in the presence of the ATP synthase inhibitor oligomycin A 1 μM.
Error bars depict SE (A) or SD (B-F). Statistical analysis was performed for each experiment on $n \geq 3$ biological replicates using a two-tailed paired t test with unequal variance. *$p<0.05$, ***$p<0.001$ represent p-values significance.

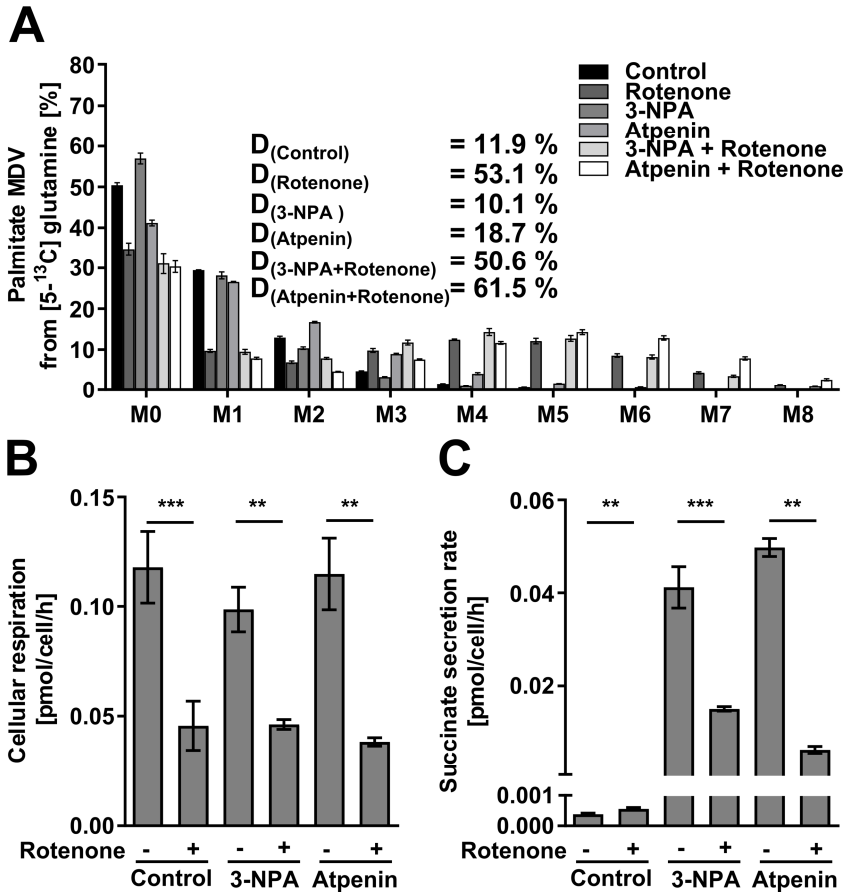

Figure 3 Dual loss of complex I and SDH activities recapitulates the metabolic phenotype of SDH mutant tumors

(A) Reductive glutamine metabolism based on the contribution of 5-^{13}C-glutamine to palmitate. D values represent the fraction of newly synthesized palmitate that was produced from reductive glutamine metabolism in DU145 prostate cancer cells treated with DMSO solvent control, 3-NPA, or Atpenin A5 with or without complex I inhibitor rotenone. All confidence intervals were ≤ 1.86%. **(B)** Cellular respiration measured in DU145 cells treated with DMSO solvent control, 3-NPA or Atpenin A5 with or without complex I inhibitor rotenone. **(C)** Succinate secretion rates measured in DU145 with DMSO solvent control, 3-NPA, or Atpenin A5 with or without complex I inhibitor rotenone, based on succinate abundance in the media after 72h treatment with the drugs. In all experiments, cells were all treated over 72h with rotenone 20 ng ml^{-1}, 3-NPA 5 mM and Atpenin A5 500 nM.

Error bars depict SD. Statistical analysis was performed for each experiment on n≥3 biological replicates using a two-tailed paired t test with unequal variance. **p<0.01, ***p<0.001 represent p-values significance.

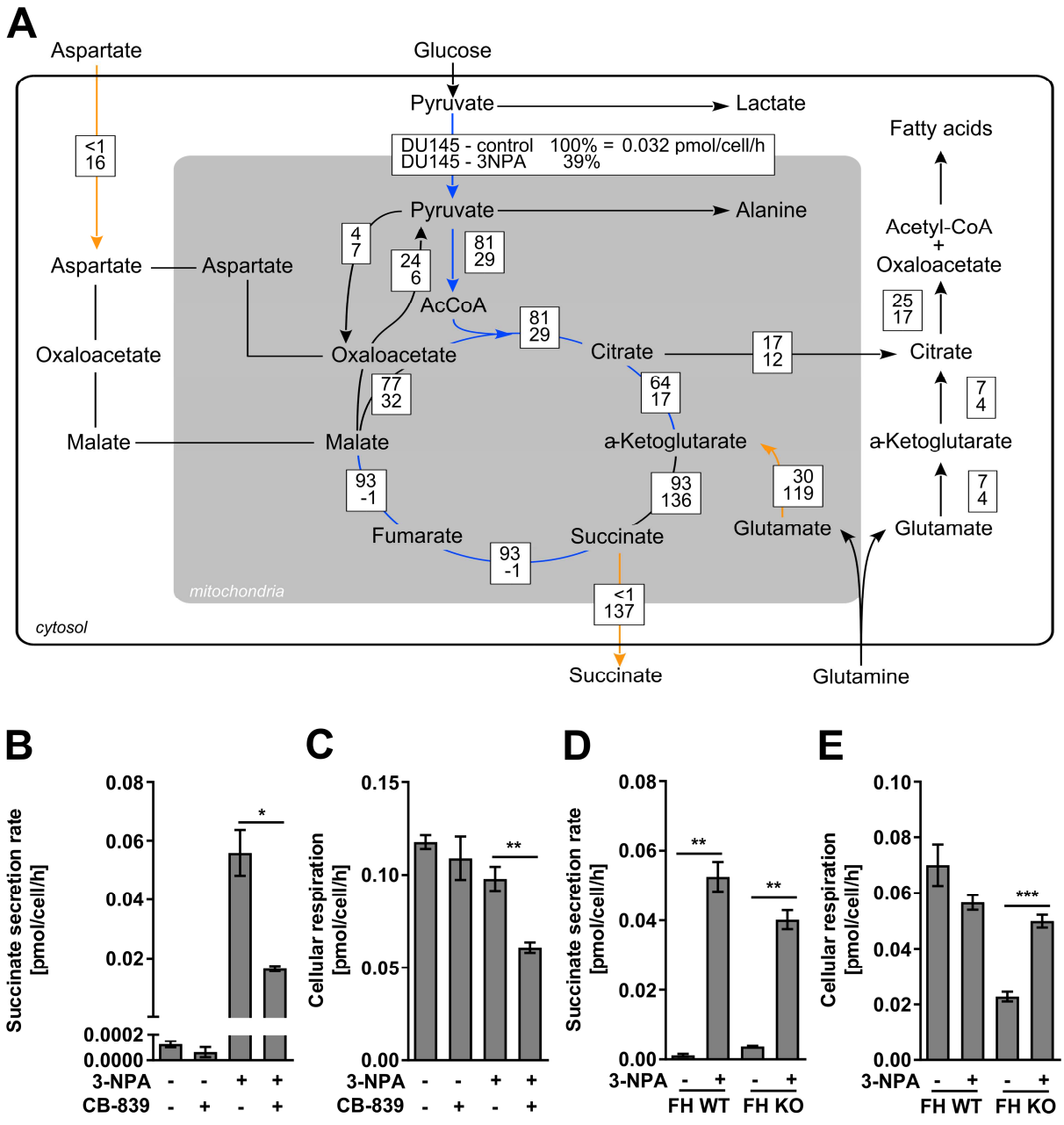

Figure 4 Succinate secretion flux is required for sustained cellular respiration upon SDHA inhibition

(A) Metabolic fluxes upon SDHA inhibition (3-NPA 5 mM) and in control (DMSO treated) condition in DU145 prostate cancer cells. Fluxes are normalized to the pyruvate entry into the mitochondria. Orange arrows indicate flux increases ≥ 2 fold in 3-NPA treated cells compared to control cells, blue arrows indicate flux decreases ≥ 2 fold in 3-NPA treated cells compared to control cells. Only selected fluxes are depicted (see Table S2 for the entirety of the estimated

fluxes). **(B-C)** Succinate secretion rates and cellular respiration in DU145 cells treated with DMSO (control condition) or 3-NPA (5 mM) in presence or absence of the glutaminase inhibitor CB-839 (100 nM). **(D-E)** Succinate secretion rates and cellular respiration in UOK262 kidney cancer cells, which are characterized by a loss of fumarate hydratase (FH) TCA cycle enzymes (FH KO), and in UOK262 control cells (FH WT) in which FH has been re-expressed, in presence and absence of 3-NPA (5 mM).

Error bars depict SD. Statistical analysis was performed for each experiment on $n \geq 3$ biological replicates using a two-tailed paired t test with unequal variance. *$p<0.05$, **$p<0.01$, ***$p<0.001$ represent p-values significance.

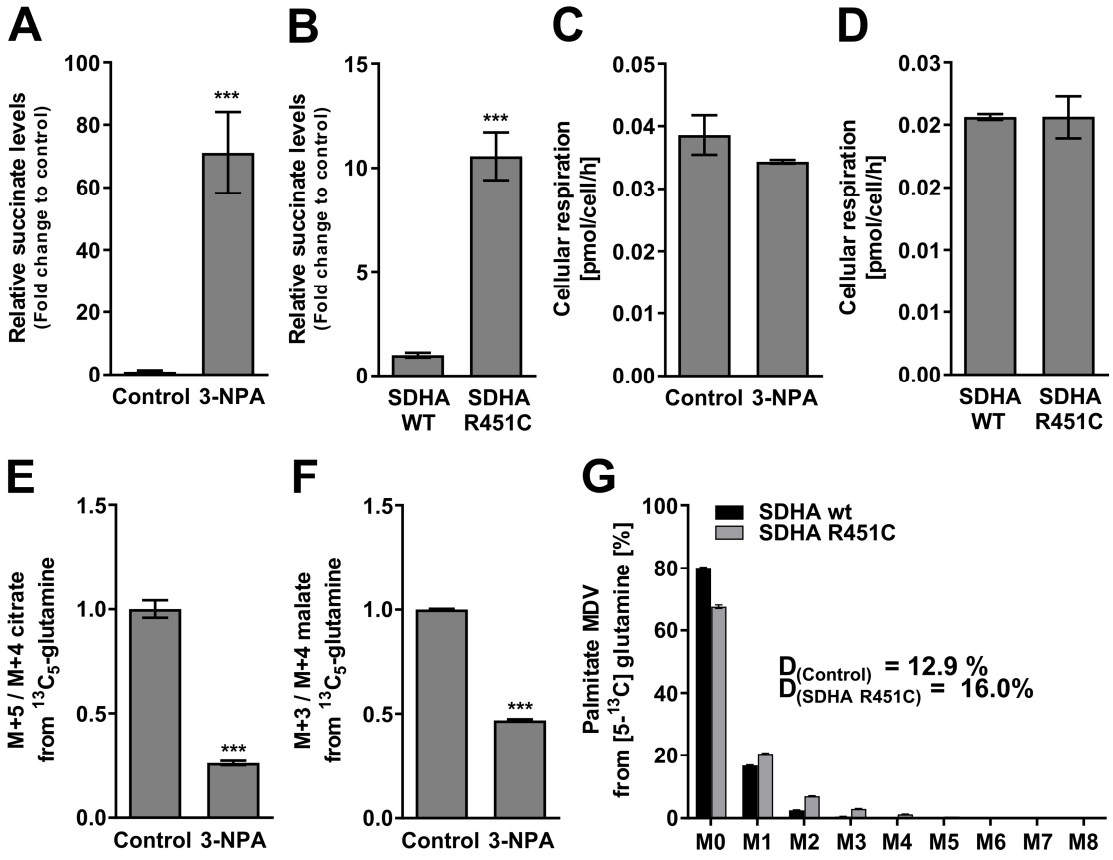

Figure 5 Neurons with SDHA inhibition and cells with neurodegeneration-associated SDHA R451C mutation show sustained cellular respiration

(A-B) Succinate levels in neurons (differentiated LUHMES cells) upon inhibition of SDHA with 3-NPA 1 mM and in Hap1 SDHA knockout (KO) cells overexpressing the SDHA R451C mutation compared to control. **(C-D)** Cellular respiration in neurons (differentiated LUHMES cells) upon inhibition of SDHA with 3-NPA 1 mM and in Hap1 SDHA knockout (KO) cells overexpressing the SDHA R451C mutation compared to control. **(E-F)** Reductive versus oxidative glutamine metabolism (M+5 / M+4 labeling of citrate from $^{13}C_5$-glutamine and M+3 / M+4 labeling of malate from $^{13}C_5$-glutamine) in differentiated LUHMES cells. **(G)** Reductive glutamine metabolism based on the contribution of 5-^{13}C-glutamine to palmitate. D values represent the fraction of newly synthesized palmitate that was produced from reductive glutamine metabolism in Hap1 SDHA KO cells overexpressing the SDHA R451C mutation and their control Hap1 SDHA KO overexpressing SDHA wt. All confidence intervals were ≤ 0.92%.

Error bars depict SD. Statistical analysis was performed for each experiment on n≥3 biological replicates using a two-tailed paired t test with unequal variance. ***p<0.001 represent p-values significance.

Supplemental Figures S1-S4 and Tables T1-T2
Lorendeau *et al.*: Dual loss of succinate dehydrogenase (SDH) and complex I activity is necessary to recapitulate the metabolic phenotype of SDH mutant tumors

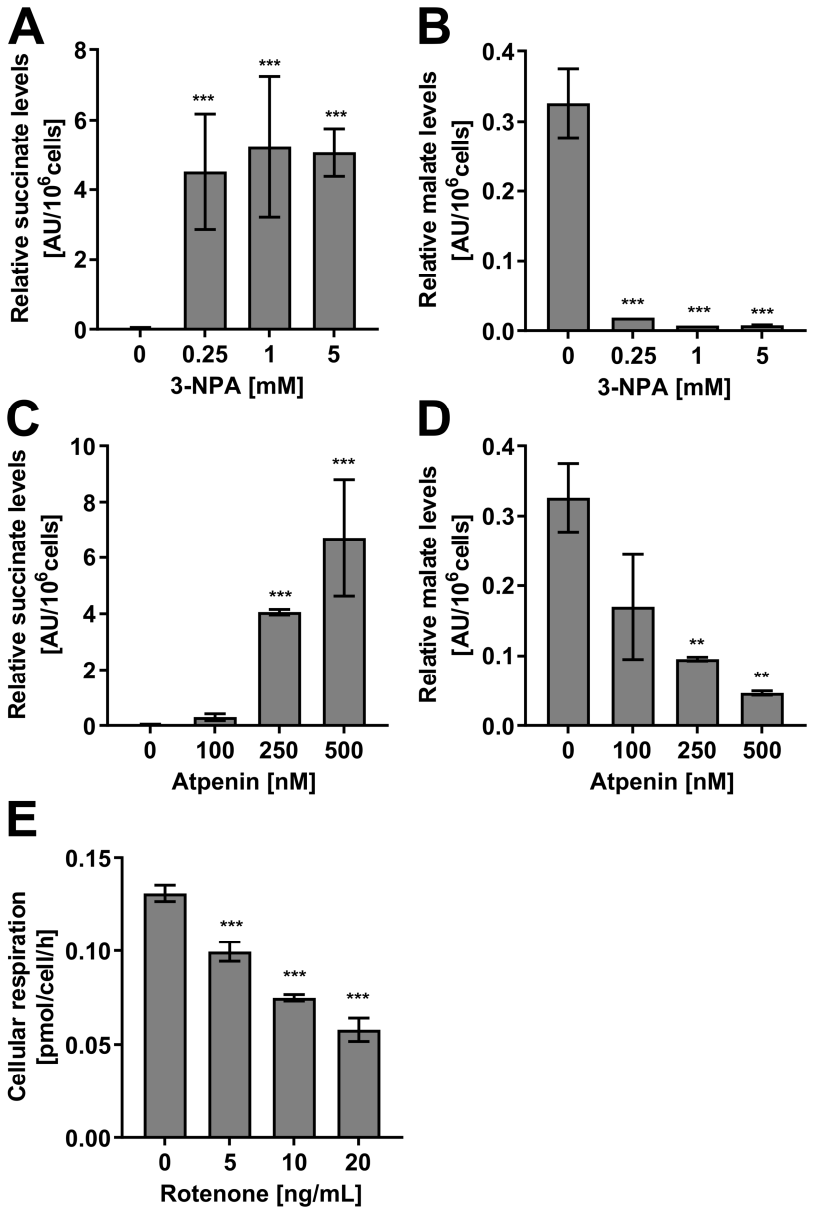

Figure S1 The SDH inhibitors 3-NPA and Atpenin A5 drastically increase succinate intracellular levels while reducing malate intracellular levels in DU145 cells.
(A-B) Relative intracellular succinate and malate levels in DU145 cells upon treatment with the SDHA inhibitor 3-NPA. (C-D) Relative intracellular succinate and malate levels in DU145 cells upon treatment with the SDHB inhibitor Atpenin A5. (E) Cellular respiration (pmol/cell/h) measured in DU145 cells treated with the complex I inhibitor rotenone. Error bars depict SD. Statistical analysis was performed on ($n \geq 3$) independent biological replicates using a two-tailed Student's t-test with unequal variance. **$p<0.01$, ***$p<0.001$ represent p-values significance.

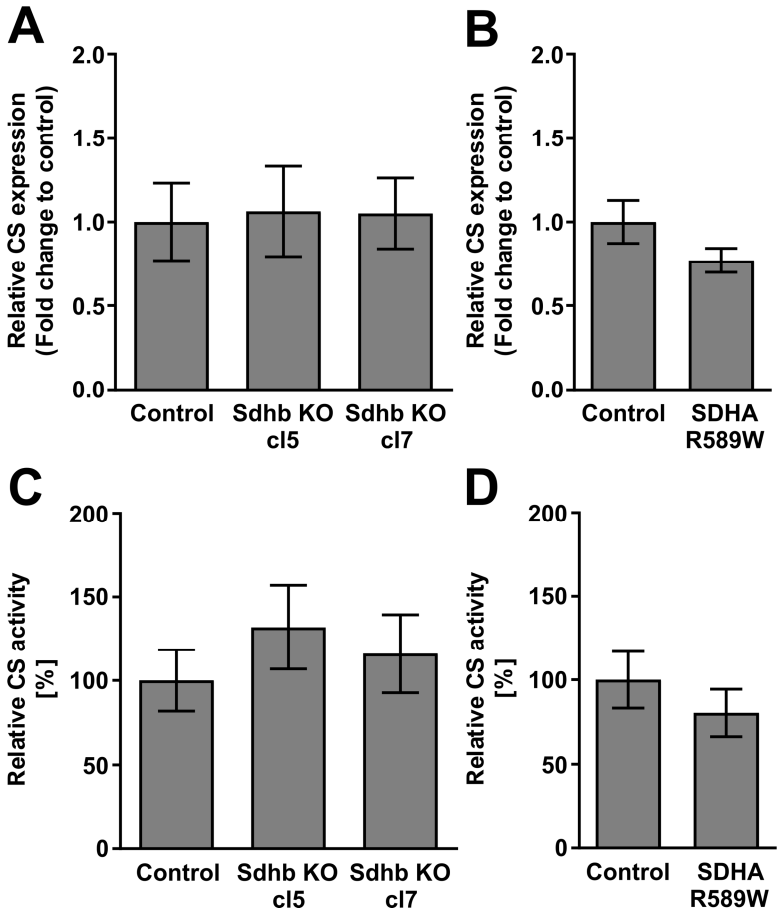

Figure S2 Relative expression and activity levels of citrate synthase (CS) in SDHB KO and SDHA R589W mutant cell lines are similar.

(A-B) Relative expression levels (mRNA) of citrate synthase (CS) in SDHB knockout (KO) mouse kidney cells and SDHA R589W Hap1 cells to control cells. (C-D) Relative CS enzymatic activity in mitochondrial fraction of SDHB KO mouse kidney cells and SDHA R589W Hap1 cells to control cells. Error bars depict SE. Statistical analysis was performed on ($n \geq 3$) independent biological replicates using a two-tailed Student's t-test with unequal variance.

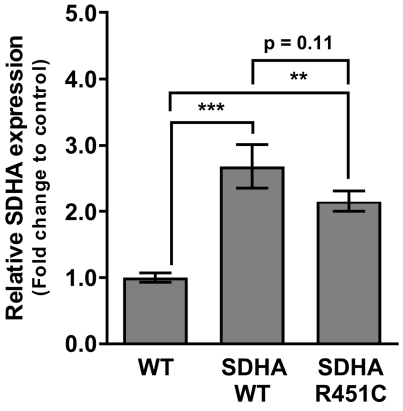

Figure S3 Relative expression of succinate dehydrogenase subunit A (SDHA) in Hap1 cell lines.

Relative expression levels (mRNA) of succinate dehydrogenase subunit A (SDHA) in Hap1 wt, Hap1 SDHA KO cells overexpressing the SDHA R451C mutation and its control Hap1 SDHA KO SDHA wt overexpressing cell line. Error bars depict SD. Statistical analysis was performed on ($n \geq 3$) independent biological replicates using a two-tailed Student's t-test with unequal variance. **$p<0.01$, ***$p<0.001$ depict p-values significance

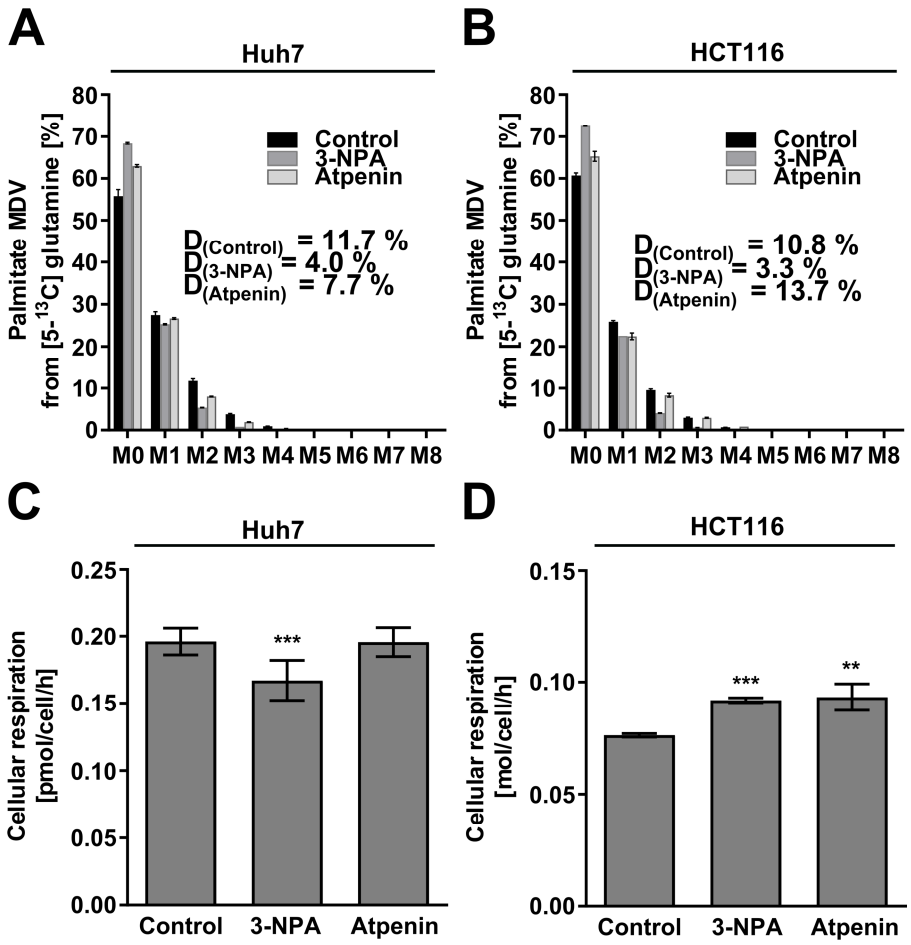

Figure S4 SDHA or B inhibition is not sufficient to induce reductive glutamine metabolism and decrease cellular respiration.

(A-B) Reductive glutamine metabolism based on the contribution of 5-^{13}C-glutamine to palmitate. D values represent the fraction of newly synthesized palmitate that was produced from reductive glutamine metabolism in Huh7 human hepatocarcinoma cells and in HCT116 human colorectal carcinoma cells treated with 3-NPA 5 mM or Atpenin A5 500nM upon incubation in medium containing 4 mM 5-^{13}C-glutamine tracer for 72h. All 95 % confidence intervals were ≤ 0.53% for ≤ 0.99% for HCT116. (C-D) Oxygen consumption rates (pmol/cell/h) measured in Huh7 and in HCT116 cells treated with 3-NPA 5 mM or Atpenin A5 500nM over 72h. Error bars depict SD. Statistical analysis was performed on (n≥3) independent biological replicates using a two-tailed Student's t-test with unequal variance comparing pharmacological inhibition with control. **p<0.01, ***p<0.001 represent p-values significance.

Table 1 Sequences of SDHA ORF cloned into the pLVX vector

ATGTCGGGGGTCCGGGGCCTGTCGCGGCTGCTGAGCGCTCGGCGCCTGGCGCTGGCCAAGGCGTGGCC
AACAGTGTTGCAAACAGGAACCCGAGGTTTTCACTTCACTGTTGATGGGAACAAGAGGGCATCTGCTA
AAGTTTCAGATTCCATTTCTGCTCAGTATCCAGTAGTGGATCATGAATTTGATGCAGTGGTGGTAGGCG
CTGGAGGGGCAGGCTTGCGAGCTGCATTTGGCCTTTCTGAGGCAGGGTTTAATACAGCATGTGTTACC
AAGCTGTTTCCTACCAGGTCACACACTGTTGCAGCACAGCTAGAAAATTATGGCATGCCGTTTAGCAG
AACTGAAGATGGGAAGATTTATCAGCGTGCATTTGGTGGACAGAGCCTCAAGTTTGGAAAGGGCGGG
CAGGCCCATCGGTGCTGCTGTGTGGCTGATCGGACTGGCCACTCGCTATTGCACACCTTATATGGAAG
GTCTCTGCGATATGATACCAGCTATTTTGTGGAGTATTTTGCCTTGGATCTCCTGATGGAGAATGGGGA
GTGCCGTGGTGTCATCGCACTGTGCATAGAGGACGGGTCCATCCATCGCATAAGAGCAAAGAACACTG
TTGTTGCCACAGGAGGCTACGGGCGCACCTACTTCAGCTGCACGTCTGCCCACACCAGCACTGGCGAC
GGCACGGCCATGATCACCAGGGCAGGCCTTCCTTGCCAGGACCTAGAGTTTGTTCAGTTCCACCCTAC
AGGCATATATGGTGCTGGTTGTCTCATTACGGAAGGATGTCGTGGAGAGGGAGGCATTCTCATTAACA
GTCAAGGCGAAAGGTTTATGGAGCGATACGCCCCTGTCGCGAAGGACCTGGCGTCTAGAGATGTGGTG
TCTCGGTCCATGACTCTGGAGATCCGAGAAGGAAGAGGCTGTGGCCCTGAGAAAGATCACGTCTACCT
GCAGCTGCACCACCTACCTCCAGAGCAGCTGGCCACGCGCCTGCCTGGCATTTCAGAGACAGCCATGA
TCTTCGCTGGCGTGGACGTCACGAAGGAGCCGATCCCTGTCCTCCCCACCGTGCATTATAACATGGGC
GGCATTCCCACCAACTACAAGGGGCAGGTCCTGAGGCACGTGAATGGCCAGGATCAGATTGTGCCCG
GCCTGTACGCCTGTGGGGAGGCCGCCTGTGCCTCGGTACATGGT**GCt**AAC**tGC**CTCGGGGCAAACTCGC
TCTTG**GAt**CTGGTTGTCTTTGGTCGGGCATGTGCCCTGAGCATCGAAGAGTCATGCAGGCCTGGAGATA
AAGTCCCTCCAATTAAACCAAACGCTGGGGAAGAATCTGTCATGAATCTTGACAAATTGAGATTTGCT
GATGGAAGCATAAGAACATCGGAACTGCGACTCAGCATGCAGAAGTCAATGCAAAATCATGCTGCCG
TGTTCCGTGTGGGAAGCGTGTTGCAAGAAGGTTGTGGGAAAATCAGCAAGCTCTATGGAGACCTAAAG
CACCTGAAGACGTTCGACCGGGGAATGGTCTGGAACACGGACCTGGTGGAGACCCTGGAGCTGCAGA
ACCTGATGCTGTGTGCGCTGCAGACCATCTACGGAGCAGAGGCACGGAAGGAGTCACGGGGCGCGCA
TGCCAGGGAAGACTACAAGGTGCGGATTGATGAGTACGATTACTCCAAGCCCATCCAGGGGCAACAG
AAGAAGCCCTTTGAGGAGCACTGGAGGAAGCACACCCTGTCCTATGTGGACGTTGGCACTGGGAAGG
TCACTCTGGAATATAGACCCGTGATCGACAAAACTTTGAACGAGGCTGACTGTGCCACCGTCCCGCCA
GCCATTCGCTCCTACTGA

Red = point mutation CTG>TTG

Green = silent mutation of PAM

Table 2 ^{13}C metabolic flux analysis in cells with and without 3-NPA treatment

		DMSO SSE = 56.0 Expected SSE = [22.9 56.9] (95% conf., 38 DOF)			3-NPA SSE = 37.4 Expected SSE = [15.3 44.5] (95% conf., 28 DOF)		
Metabolic reaction	**Description**	**Flux [pmol/cell/h]**	**95% conf. min**	**95% conf. max**	**Flux [pmol/cell/h]**	**95% conf. min**	**95% conf. max**
R1	Gluc.x -> G6P	0.601	0.5873	0.6158	0.812	0.7063	0.9175
R2 net	G6P -> F6P	0.6264	0.6264	0.642	0.8374	0.7281	0.9466
R2 exch	G6P <-> F6P	1.00E-07	0	Inf	0.5803	0	Inf
R3	F6P -> DHAP + GAP	0.6265	0.6113	0.6414	0.8374	0.7282	0.9466
R4 net	DHAP -> GAP	0.6265	0.6113	0.6414	0.8374	0.7282	0.9466
R4 exch	DHAP <-> GAP	0.2232	0	Inf	0.4433	0	Inf
R5 net	GAP -> 3PG	1.25	1.223	1.283	1.675	1.456	1.893
R5 exch	GAP <-> 3PG	0.3053	0	Inf	0.593	0	Inf
R6	3PG -> Pyr.c	1.246	1.216	1.276	1.673	1.455	1.892
R7 net	Pyr.c -> Lac	1.177	1.148	1.205	1.657	1.44	1.875
R7 exch	Pyr.c <-> Lac	0.0005601	0	Inf	0.1357	0	Inf
R8	Lac -> Lac.x	1.177	1.148	1.205	1.657	1.44	1.875
R9 net	DHAP -> GLP	0	0	0	-1.11E-16	0	0
R9 exch	DHAP <-> GLP	1.66	0	Inf	0.2889	0	Inf
R10 net	GLP -> GLP.x	0	0	0	-1.11E-16	0	0
R10 exch	GLP <-> GLP.x	2.506	0	Inf	0.6478	0	Inf
R11	G6P -> 6PG	0.005131	0	0.01493	0.001201	0	0.003553
R12	6PG -> P5P + CO2	0.005131	0	0.01493	0.001201	0	0.003553
R13 net	P5P + P5P -> S7P + GAP	4.15E-05	-0.001943	0.003323	2.08E-07	-0.000467	0.000788
R13 exch	P5P + P5P <-> S7P + GAP	1.00E-07	0	Inf	3.229	0	Inf
R14 net	S7P + GAP -> F6P + E4P	4.15E-05	-0.001943	0.003323	2.08E-07	-0.000467	0.000788
R14 exch	S7P + GAP <-> F6P + E4P	0.7496	0	Inf	0.1869	0	Inf
R15 net	P5P + E4P -> F6P + GAP	4.15E-05	-0.001943	0.003323	2.08E-07	-0.000467	0.000788
R15 exch	P5P + E4P <-> F6P + GAP	0.03613	0	0.1835	2.15E-05	0	0.9385
R16	Pyr.m + CO2 -> Oac.m	0.0012	0.000916	0.001572	0.002394	0.001306	0.01991
R17	Mal.m -> Pyr.m + CO2	0.00764	0.007059	0.01568	0.001821	0.0009102	0.07655
R18	Pyr.m -> AcCoA.m + CO2	0.02598	0.02364	0.02998	0.009331	0.007259	0.01208
R19	AcCoA.m + Oac.m -> Cit.m	0.02598	0.02338	0.02948	0.009332	0.006997	0.01213
R20	Cit.m -> Akg.m + CO2	0.02047	0.01851	0.02361	0.005402	0.003422	0.007986
R21	Akg.m -> Suc + CO2	0.03014	0.02754	0.04081	0.04387	0.03798	0.0498
R22 net	Suc -> Fum.m	0.03012	0.0275	0.0408	-0.0002563	-0.004133	0.002954
R23 exch	Fum.m <-> Mal.m	0.07569	0	Inf	0.00128	0	0.1475

		DMSO			3-NPA		
Metabolic reaction	**Description**	**Flux [pmol/cell/h]**	**95% conf. min**	**95% conf. max**	**Flux [pmol/cell/h]**	**95% conf. min**	**95% conf. max**
R24 net	Mal.m -> Oac.m	0.02478	-0.00326	0.03588	0.01022	-0.008623	0.032
R24 exch	Mal.m <-> Oac.m	0.1353	0.02613	Inf	0.01378	0	Inf
R25	Cit.m -> AcCoA.c + Oac.c	0.005514	0.00388	0.007111	0.003929	0.002891	0.004972
R26	Cit.c -> AcCoA.c + Oac.c	0.002395	0.001956	0.002861	0.001389	0.001122	0.001597
R27 net	Fum.c -> Mal.c	892.2	0	> 4.653e+06	1.01E-07	0	0.09592
R27 exch	Fum.c <-> Mal.c	654.4	0	Inf	0.004953	0	0.1479
R28 net	Mal.c -> Oac.c	892.2	-0.002296	> 4.182e+05	-0.01229	-0.1065	-0.004283
R28 exch	Mal.c <-> Oac.c	1.00E-07	0	Inf	0.001687	0	Inf
R29 net	Oac.c -> Asp.c	892.2	-0.01308	> 3.875e+05	-0.006975	-0.02804	0.03918
R29 exch	Oac.c <-> Asp.c	1.00E-07	0	Inf	1.00E-07	0	Inf
R30	Asp.c -> Fum.c	892.2	0	> 4.653e+06	1.01E-07	0	0.09592
R31	AcCoA.c -> FA	0.007909	0.006342	0.009468	0.005318	0.004313	0.006356
R32 net	Pyr.m -> Ala	0.01271	0.0115	0.01391	0.002799	0.002186	0.003411
R32 exch	Pyr.m <-> Ala	0.3269	0	Inf	0.2426	0	Inf
R33 net	Oac.m -> Asp.m	-4.44E-16	-0.0281	0.02339	0.003278	-0.01371	0.04433
R33 exch	Oac.m <-> Asp.m	0.2243	0	Inf	1.00E-07	0	Inf
R34	Gln.x -> Gln	0.0385	0.0352	0.04572	0.04725	0.04132	0.05316
R35 net	Gln -> Glu	0.03719	0.03382	0.04443	0.04695	0.041	0.05291
R35 exch	Gln <-> Glu	0.07891	0.03893	0.206	0.6956	0.03234	Inf
R36	Glu -> Glu.x	0.02323	0.01973	0.02628	0.006691	0.0003776	0.01302
R37 net	Glu -> Akg.m	0.009672	0.00844	0.0176	0.03847	0.03267	0.04443
R37 exch	Glu <-> Akg.m	2.923	0.8564	Inf	0.2034	0.04485	Inf
R38 net	Glu -> Akg.c	0.002395	0.001956	0.002861	0.001389	0.001122	0.001597
R38 exch	Glu <-> Akg.c	0.6509	0	Inf	1.838	0	Inf
R39	Akg.c + CO2 -> Cit.c	0.002395	0.001956	0.002861	0.001389	0.001122	0.001597
R40	Asp.c -> Biomass	0.003108	0.002501	0.003703	0.0008	0.0006434	0.000956
R41	Glu -> Biomass	0.001903	0.00153	0.002273	0.0003993	0.0003215	0.000478
R42	Ala -> Biomass	0.003603	0.002898	0.004307	0.0008999	0.0007236	0.001076
R43	Gln -> Biomass	0.001301	0.001046	0.001555	0.0002996	0.0002427	0.000358
R44	Asp.c -> NTP + CO2	0.002505	0.002015	0.002987	0.0006	0.0004825	0.000717
R45	P5P -> NTP	0.005007	0.004027	0.005983	0.0012	0.0009647	0.001435
R46	3PG -> Ser	0.006707	0.005394	0.00802	0.0013	0.001045	0.001555
R47	Ala -> Ala.x	0.009107	0.008127	0.01008	0.001899	0.001312	0.002487

		DMSO			3-NPA		
Metabolic reaction	**Description**	**Flux [pmol/cell/h]**	**95% conf. min**	**95% conf. max**	**Flux [pmol/cell/h]**	**95% conf. min**	**95% conf. max**
R48	Asp.x -> Asp.c	1.00E-07	0	0.001189	0.005097	0.001435	0.02341
R49	Pyr.c -> Pyr.x	0.03758	0.02799	0.04715	0.003499	0.001931	0.005067
R50	Suc -> Suc.x	1.28E-05	0	0.000403	0.04413	0.03763	0.0509
R51 net	Pyr.c -> Pyr.m	0.03225	0.0271	0.0343	0.0127	-0.04505	0.01573
R51 exch	Pyr.c <-> Pyr.m	1.00E-07	0	0.0384	1.00E-07	0	0.736
R52	0*Pyr.c -> Pyr.mnt	1	0	1	0.3101	0	1
R53	0*Pyr.m -> Pyr.mnt	1.00E-07	0	1	0.6899	0	1
R54	Pyr.mnt -> Pyr.fix	1	1	1	1	1	1
R55	0*Cit.c -> Cit.mnt	0.1066	0.08387	0.1166	0.398	0.3087	0.4852
R56	0*Cit.m -> Cit.mnt	0.8934	0.8834	0.9161	0.602	0.5148	0.6913
R57	Cit.mnt -> Cit.fix	1	1	1	1	1	1
R58	0*Fum.c -> Fum.mnt	0.701	0	1	0.2817	0	1
R59	0*Fum.m -> Fum.mnt	0.299	0	1	0.7183	0	1
R60	Fum.mnt -> Fum.fix	1	1	1	1	1	1
R61	0*Akg.c -> Akg.mnt	1	0	1	0.3057	0	1
R62	0*Akg.m -> Akg.mnt	1.00E-07	0	1	0.6943	0	1
R63	Akg.mnt -> Akg.fix	1	1	1	1	1	1
R64 net	Mal.c -> Mal.m	0.002296	-0.02593	0.01811	0.01229	-0.002543	0.09538
R64 exch	Mal.c <-> Mal.m	0.01674	0	0.03743	56.12	0	Inf
R65	0*Mal.c -> Mal.mnt	0.7169	0.222	1	1	0	1
R66	0*Mal.m -> Mal.mnt	0.2831	0	0.778	1.01E-07	0	1
R67	Mal.mnt -> Mal.fix	1	1	1	1	1	1
R68 net	Asp.c -> Asp.m	2.36E-16	-0.02339	0.0281	-0.003278	-0.04433	0.01371
R68 exch	Asp.c <-> Asp.m	1.00E-07	0	0.01865	0.6969	0	Inf
R69	0*Asp.c -> Asp.mnt	1	0.328	1	0.9864	0	1
R70	0*Asp.m -> Asp.mnt	1.00E-07	0	0.672	0.01364	0	1
R71	Asp.mnt -> Asp.fix	1	1	1	1	1	1
R72	UnlabeledAcCoA.x -> AcCoA.m	1.00E-07	0	0.000622	1.00E-07	0	0.000239
R73	UnlabeledC.x -> G6P	0.03056	0.02623	0.03334	0.02655	0	0.03241